

INFORMATION TO USERS

This manuscript has been reproduced from the microfilm master. UMI films the text directly from the original or copy submitted. Thus, some thesis and dissertation copies are in typewriter face, while others may be from any type of computer printer.

The quality of this reproduction is dependent upon the quality of the copy submitted. Broken or indistinct print, colored or poor quality illustrations and photographs, print bleedthrough, substandard margins, and improper alignment can adversely affect reproduction.

In the unlikely event that the author did not send UMI a complete manuscript and there are missing pages, these will be noted. Also, if unauthorized copyright material had to be removed, a note will indicate the deletion.

Oversize materials (e.g., maps, drawings, charts) are reproduced by sectioning the original, beginning at the upper left-hand corner and continuing from left to right in equal sections with small overlaps.

**ProQuest Information and Learning
300 North Zeeb Road, Ann Arbor, MI 48106-1346 USA
800-521-0600**

UMI[®]

University of Alberta

**Ultra-Flat Self-Assembled Monolayer (SAM) Surfaces Formed on
Annealed and Template-Stripped Gold (Au) Substrates**

by

Kelvin Isaacson ©

A thesis submitted to the Faculty of Graduate Studies and Research in partial
fulfillment of the requirements for the degree of **Master of Science**.

Department of Mechanical Engineering

Edmonton, Alberta

Spring 2005



Library and
Archives Canada

Bibliothèque et
Archives Canada

Published Heritage
Branch

Direction du
Patrimoine de l'édition

395 Wellington Street
Ottawa ON K1A 0N4
Canada

395, rue Wellington
Ottawa ON K1A 0N4
Canada

Your file *Votre référence*

ISBN:

Our file *Notre référence*

ISBN:

NOTICE:

The author has granted a non-exclusive license allowing Library and Archives Canada to reproduce, publish, archive, preserve, conserve, communicate to the public by telecommunication or on the Internet, loan, distribute and sell theses worldwide, for commercial or non-commercial purposes, in microform, paper, electronic and/or any other formats.

The author retains copyright ownership and moral rights in this thesis. Neither the thesis nor substantial extracts from it may be printed or otherwise reproduced without the author's permission.

AVIS:

L'auteur a accordé une licence non exclusive permettant à la Bibliothèque et Archives Canada de reproduire, publier, archiver, sauvegarder, conserver, transmettre au public par télécommunication ou par l'Internet, prêter, distribuer et vendre des thèses partout dans le monde, à des fins commerciales ou autres, sur support microforme, papier, électronique et/ou autres formats.

L'auteur conserve la propriété du droit d'auteur et des droits moraux qui protègent cette thèse. Ni la thèse ni des extraits substantiels de celle-ci ne doivent être imprimés ou autrement reproduits sans son autorisation.

In compliance with the Canadian Privacy Act some supporting forms may have been removed from this thesis.

Conformément à la loi canadienne sur la protection de la vie privée, quelques formulaires secondaires ont été enlevés de cette thèse.

While these forms may be included in the document page count, their removal does not represent any loss of content from the thesis.

Bien que ces formulaires aient inclus dans la pagination, il n'y aura aucun contenu manquant.


Canada

"I like nonsense, it wakes up the brain cells. Fantasy is a necessary ingredient in living, it's a way of looking at life through the wrong end of a telescope. Which is what I do, and that enables you to laugh at life's realities."

-Dr. Suess

"Leave the beaten track occasionally and dive into the woods. Every time you do you will be certain to find something you have never seen before."

-Alexander Graham Bell

To my colleagues: I've enjoyed doing science with you!

ABSTRACT

Self-Assembled Monolayers (SAMs) have attracted a great deal of attention due to their potential to be used in molecular assembly. In the literature the most popular choice of substrate for -thiol monolayers is an evaporated gold substrate, generally on a Si wafer with either a Ti or Cr adhesion layer. However, even as smooth as evaporated surfaces are, they still generate fairly rough surfaces in molecular terms and since SAMs are typically monomolecular, this roughness does affect the SAM interface. The effect of this substrate roughness on the monolayer interface is investigated with various techniques: Atomic Force Microscopy (AFM), Spectroscopic Ellipsometry, Fourier Transform Infrared (FT-IR) and low rate dynamic contact angles measured with axisymmetric drop shape analysis - profile (ADSA-P) technique. Finally a model is proposed to explain the experimental data.

ACKNOWLEDGEMENTS

I would like to start by thanking my family (you know who you are!) who were supportive the whole way.

The second most important people I would like to thank are the teachers who encouraged my curiosity rather than squelching it: from Mallaig Community School there were Mr. Mottus and Mr. Wilson in particular, and here at the University, almost every professor has given me inspiration of one form or another. On top of the list is my supervisor Dr. Daniel Y. Kwok.

I would also like to make mention of my lab colleagues: Ali, Gill, Lu, Maggie, Yu-Wen, Gary, Steven, Jeff, C.J., Scott and Tian. You made it a fun environment to learn and experiment in - it would have been a lot duller place without you.

Special thanks to all the machinists and technicians: Albert Yeun, Dave Pape, Terri Nord, Tulla Hilvo, Bernie Faulkner, Andrew Coward and Ian Buttar whose knowledge and abilities helped me a great deal.

TABLE OF CONTENTS

1	Introduction	1
2	Literature Review	5
2.1	SAMs on Evaporated Surfaces	5
2.1.1	History	5
2.1.2	Alkanethiol SAMs	6
2.1.3	Atomic Force Microscopy (AFM)	8
2.1.4	Spectroscopic Ellipsometry	8
2.1.5	Fourier Transform Infrared (FT-IR)	9
2.1.6	Advancing Contact Angle	13
2.1.7	Contact Angle Hysteresis	15
2.1.8	Contact Angle Interpretation	15
2.2	Flat substrates	18
2.2.1	Ultraflat Template-stripped Surfaces	18
3	Experimental Setup	21
3.1	Materials	21
3.2	Preparation of Evaporated and Annealed SAMs.	23

3.3	Preparation of Template-Stripped SAMs.	23
3.4	Characterization of SAMs.	25
3.4.1	AFM — Evaporated and Annealed Samples	25
3.4.2	AFM — Template Stripped Samples	25
3.4.3	Spectroscopic Ellipsometry	26
3.4.4	FT-IR	27
3.4.5	Contact Angle Measurements	28
4	Results	32
4.1	AFM	32
4.1.1	Evaporated Au	32
4.1.2	Annealed Au	32
4.1.3	Template-Stripped Au	32
4.1.4	Comparison of AFM images for evaporated, annealed, and template-stripped Au samples	33
4.2	Spectroscopic Ellipsometry Data	34
4.2.1	Octadecanethiol SAMs on Evaporated, Annealed and Tem- plate-stripped Au	34
4.2.2	Dodecanethiol SAMs on Template-stripped Au	35
4.3	FT-IR data	35
4.3.1	Octadecanethiol Monolayers on Evaporated, Annealed and Template-stripped Au	35
4.3.2	Dodecanethiol Monolayers on Template-stripped Au	38
4.4	Contact Angle Data	38

4.4.1	Octadecanethiol on Evaporated, Annealed and Template-stripped Au	38
4.4.2	Dodecanethiol on Template-stripped Au	41
5	Discussion	55
6	Conclusions and Future Work	70
6.1	Conclusion	70
6.2	Future Work	71
	Bibliography	72

LIST OF TABLES

2.1	Peak positions for SH(CH ₂) _{n-1} CH ₃ C-H stretching modes for crystalline state, liquid state and adsorbed onto Au substrate and the assigned direction of the transition dipole (reproduced from [1, 2]). Note that n = total number of carbon atoms in the molecule.	12
2.2	Contact angle hysteresis (H) in degrees (°) for SH(CH ₂) _{n-1} CH ₃ adsorbed onto Au for water (H ₂ O) and hexadecane (HD). Data from [2-5] ^a	17
3.1	Experimental liquid-vapor surface tensions ^a determined via pendant drop method (ADSA-P) [6-8]	22
4.1	Spectroscopic ellipsometric thickness measurements of octadecanethiol adsorbed on evaporated, annealed, and template-stripped Au.	34
4.2	A comparison of advancing contact angles (deg.) on octadecanethiol monolayers formed on: template-stripped Au (TS), annealed Au (A) and evaporated Au (E). Errors shown are the 95% confidence limits.	39

4.3	Experimental contact angle hysteresis (H) on SAMs of octadecanethiol adsorbed onto template-stripped Au (TS), annealed Au (A), and evaporated Au (E). Errors shown are the 95% confidence limits.	40
4.4	A comparison of advancing contact angles for octadecanethiol (C18-TS) and dodecanethiol (C12-TS) monolayers formed on template-stripped Au. For reference θ_a on evaporated monolayers is shown for both octadecanethiol (C18-E) and dodecanethiol (C12-E). Errors shown are the 95% confidence limits.	41
4.5	A comparison of advancing contact angles and contact angle hysteresis of octadecanethiol (C18-TS) and dodecanethiol (C12-TS) monolayers formed on template-stripped Au. For reference hysteresis on evaporated monolayers is shown for both octadecanethiol (C18-E) and dodecanethiol (C12-E). Errors shown are the 95% confidence limits.	42
5.1	γ_{sv} calculated using the equation of state approach with $\beta = 0.0001247 \text{ (m}^2/\text{mJ)}^2$	68

LIST OF FIGURES

1.1	Equilibrium of these interfacial tensions as derived by Young. . .	1
2.1	Schematic of a typical self-assembled organic monolayer adsorbed onto a metal substrate.	6
2.2	Schematic of the alkanethiol molecule adsorbed on Au. In this case, the terminal functional group shown is the methyl (CH ₃) molecule.	7
2.3	Ellipsometric thicknesses reported for SH(CH ₂) _{n-1} CH ₃ (alkanethiols) in [9] (■, as an estimated average thickness) and [10] (○, as an estimated thickness). The solid line represents the limiting case of a fully extended <i>all-trans</i> molecule (calculated by Eq.(2.1)) and the dotted line is the monolayer at a 30° tilt. The dashed line is provided as an aid to the eye to estimate the slope of the experimental data. Error bars (± 0.1 nm) are due to estimation of thicknesses from figures in [9, 10].	10

2.4	Typical curve for advancing contact angles of water on alkanethiols adsorbed on Au reported in literature for the different chain lengths, $\text{SH}(\text{CH}_2)_{n-1}\text{CH}_3$. Plotted values (\circ) come from [4], (\square) from [9] and (\diamond , method B where possible) from [10]. The dotted line is \sim the highest reported contact angle on a methyl (CH_3) terminated surface ([5, 11] and results shown here). The error bars ($\pm 2^\circ$) are due to the goniometer error [12]. Note the quoted reproducibility in [4] is $\pm 3^\circ$	14
2.5	(a) The solid-liquid work of adhesion W_{sl} , (b) the cosine of the contact angle, $\cos \theta$, and (c) the liquid-vapor surface tension times the cosine of the contact angle, $\gamma_{lv} \cos \theta$, versus the liquid vapor surface tension, γ_{lv} . Data shown for fluorocarbon FC722 (\square), hexatriacontane (\diamond), cholesteryl acetate (\blacklozenge), poly(<i>n</i> -butyl methacrylate) (Δ), poly(methyl methacrylate/ <i>n</i> -butyl methacrylate) (\blacktriangle), and poly (methyl methacrylate) (\blacktriangleleft) surfaces	16
2.6	A comparison of the CH_3 terminated polymer hexatriacontane (\diamond [13]) with literature data for CH_3 terminated alkanethiols (\blacktriangleleft [10], \circ [9], and \blacktriangle [4]). (a) The solid-liquid work of adhesion W_{sl} , (b) the cosine of the contact angle, $\cos \theta$, and (c) the liquid-vapor surface tension times the cosine of the contact angle, $\gamma_{lv} \cos \theta$, versus the liquid vapor surface tension, γ_{lv}	19
3.1	Sessile drop experimental setup used to capture images to be analyzed with ADSA-P.	29

4.1	1 μm AFM scan size and a zoomed in 0.3875 μm scan size of evaporated Au (~ 100 nm) Ti adhesion layer (~ 10 nm) on Si substrate.	43
4.2	1 μm AFM scan size of annealed Au (~ 100 nm) on Ti adhesion layer (~ 10 nm) on Si substrate.	44
4.3	1 μm scan size AFM images of template-stripped Au (angle and top view)	45
4.4	FT-IR spectra of octadecanethiol monolayers formed on template-stripped, annealed and evaporated Au. Peak positions: $\nu_a(\text{CH}_2)$ 2918 cm^{-1} , $\nu_s(\text{CH}_2)$ 2850 cm^{-1} , $\nu_a(\text{CH}_3)$ 2878 cm^{-1} (2877 cm^{-1} for the template-stripped sample) and $\nu_a(\text{CH}_3)$ 2965 cm^{-1} (2963 cm^{-1} for the template-stripped sample). The Fermi peak (ν_s , CH_3) is at 2938 cm^{-1} for the evaporated sample and 2940 cm^{-1} for the annealed and template-stripped samples. The spectra have been baseline corrected and offset for clarity.	46
4.5	A comparison of liquid and crystalline monolayer spectra for: (a) $\text{CH}_3(\text{CH}_2)_{11}\text{SH}$, and (b) $\text{CH}_3(\text{CH}_2)_{17}\text{SH}$. The spectra have been baseline corrected and scaled to allow comparison.	47
4.6	A simplified model used to estimate the <i>average</i> tilt of the alkanethiol monolayer using a modified version of Debe's [14] RATIO method.	48
4.7	Result for modified Debe RATIO method for monolayers adsorbed on evaporated, annealed and template-stripped Au. . . .	49

4.8	FT-IR spectra of octadecanethiol and dodecanethiol monolayers formed on template-stripped Au. The spectra have been baseline corrected and offset for clarity.	50
4.9	Typical advancing low-rate dynamic contact angle, θ_a , results for water on octadecanethiol monolayers formed on evaporated Au. As indicated in Fig.4.11(a) the mean values are taken once γ_{lv} and θ are constant.	51
4.10	Typical advancing low-rate dynamic contact angle, θ_a , results for water on octadecanethiol monolayers formed on annealed Au. As indicated in Fig.4.11(a) the mean values are taken once γ_{lv} and θ are constant.	52
4.11	Typical low-rate dynamic advancing contact angle θ_a results for water on Octadecanethiol monolayers formed on template-stripped Au. As indicated the mean values are taken once γ_{lv} and θ are constant. It is clear that, as per the conditions set out earlier, at this point θ is constant as the drop volume (V) increases and the contact line radius (R) increases steadily.	53

4.12	Typical low-rate dynamic receding contact angle θ_r results for water on Octadecanethiol monolayers formed on template-stripped Au. As indicated in Fig.4.11(a) the mean values are taken once γ_{lv} and θ are constant. It is clear that, as per the conditions set out earlier, at this point θ is constant as the drop volume (V) increases and the contact line radius (R) increases steadily. Note that, in this case, clear ‘slip-stick’ behavior (x-axis: 55–61) is demonstrated which must not be included when the contact angle is calculated — as noted earlier.	54
5.1	Advancing contact angles (θ_a) for two maleimide copolymers: [1] poly(propene- <i>alt</i> -N-(<i>n</i> -alkyl)maleimides) or (PAlkMI) [2] poly(styrene- <i>alt</i> -N-(<i>n</i> -alkyl)maleimides), (SAlkMI) versus the reciprocal of the number of CH ₂ in the side chain, x	57
5.2	A schematic illustrating how the change in the surface structure changes the solid-liquid interfacial tension, γ_{sl} . Given that γ_{sv} and γ_{lv} remain unchanged the contact angle must increase due to $\Delta\gamma_{sl}$	58
5.3	A model illustrating the differences between monolayers ($n \geq 12$) formed on evaporated Au. The y-dimension is to scale, i.e. step height to molecule length, and molecules are tilted at 30° relative to surface normal. The x-direction is not to scale between the substrate and the SAM as it is not possible to fit the number of molecules required to accurately represent the SAM.	61

5.4	A model illustrating the differences between monolayers ($n \geq 12$) formed on template-stripped and annealed Au. The y-dimension is to scale, i.e. step height to molecule length, and molecules are tilted at 30° relative to surface normal. The x-direction is not to scale between the substrate and the SAM as it is not possible to fit the number of molecules required to accurately represent the SAM.	62
5.5	(a) The solid-liquid work of adhesion, W_{sl} , (b) the cosine of the contact angle, $\cos \theta$, and (c) the liquid-vapor surface tension times the cosine of the contact angle, $\gamma_{lv} \cos \theta$, versus the liquid vapor surface tension, γ_{lv} shown for hexatriacontane (\diamond) and SAMs of octadecanethiol (\blacksquare) and dodecanethiol (\blacktriangle) formed on evaporated Au. Data for dodecanethiol shown here is calculated from [5].	66
5.6	(a) The solid-liquid work of adhesion, W_{sl} , (b) the cosine of the contact angle, $\cos \theta$, and (c) the liquid-vapor surface tension times the cosine of the contact angle, $\gamma_{lv} \cos \theta$, versus the liquid vapor surface tension, γ_{lv} . Data shown for hexatriacontane (\diamond) and octadecanethiol formed on annealed Au (\bullet) are compared to SAMs of octadecanethiol (\blacktriangleleft) and dodecanethiol (\blacktriangle) formed on template-stripped Au.	67

NOMENCLATURE

LATIN SYMBOLS

ADSA-P Axisymmetric Drop Shape Analysis - Profile

AFM.....Atomic Force Microscopy

Ag Silver

ATR Attenuated Total Reflection

Au Gold

CH₂.....Methylene

CH₃.....Methyl

CH₃(CH₂)₁₁SH Dodecanethiol

CH₃(CH₂)₁₇SH Octadecanethiol

Cu Copper

FT-IR.....Fourier Transform Infrared

GaAs.....Gallium Arsenide

H contact angle hysteresis

H₂O water

HD hexadecane

Hg Mercury

InP Indium Phosphide

IR infrared

KBr Potassium Bromide

LB Langmuir-Blodgett

N₂ Nitrogen

Pd Palladium

PV peak-to-valley

rms root-mean-square

SAM Self-Assembled Monolayer

Si Silicon

STM Scanning Tunneling Microscopy

Ti Titanium

GREEK SYMBOLS

α projected angle in the x - y plane

γ_{sv} solid-vapor surface tension

γ_{sl} solid-liquid surface tension

γ_{lv} liquid-vapor surface tension

θ_a advancing contact angle

θ_r receding contact angle

θ_Y Young's contact angle

θ tilt angle with respect to surface normal

ν_a asymmetric bond

ν_s symmetric bond

Ψ angle of rotation about the molecular axis

CHAPTER 1

INTRODUCTION

Solid-vapor (γ_{sv}) and solid-liquid (γ_{sl}) interfacial tensions can be determined via a relation of the form (that Young [15] recognized in 1805)

$$\gamma_{lv} \cos \theta_Y = \gamma_{sv} - \gamma_{sl} \quad (1.1)$$

where γ_{lv} , γ_{sv} , γ_{sl} are the interfacial tensions of the liquid-vapor, solid-vapor, and solid-liquid respectively and θ_Y is the (Young's) contact angle. The mechanical equilibrium of these interfacial tensions is illustrated in Fig. 1.1. The key

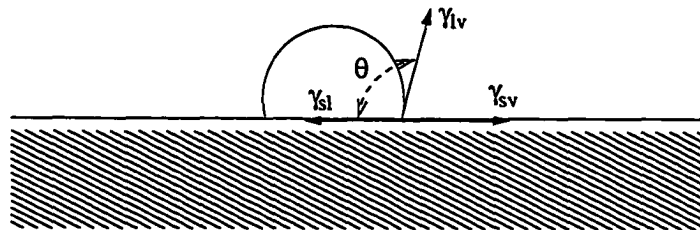


Figure 1.1: Equilibrium of these interfacial tensions as derived by Young.

assumption in deriving this relation is that the surface is idealized as a smooth, chemically homogeneous surface. Thus a 'perfect' Young's surface should always exhibit the same contact angle since γ_{lv} , γ_{sv} , and γ_{sl} (in Eq.(1.1)) are thermodynamic properties of the solid and liquid. However, in practice the advancing

(θ_a) and receding contact (θ_r) angles of a liquid on a surface are not identical; in addition many metastable contact angles exist which are not equal to θ_Y in Eq.(1.1) [16]. Several contact angle approaches of current interest [17–24] are inspired by using Young’s equation (Eq.(1.1)) to determine surface energetics. While these approaches are logically and conceptually mutually exclusive, they share the same basic assumptions:

1. All approaches assume the validity of Young’s equation in determining surface energetics from experimental contact angles.
2. Pure liquids are always used since surfactant solutions and mixtures of liquids can introduce complications due to preferential adsorption.
3. The values of γ_{lv} , γ_{sv} and γ_{sl} are assumed to be constant during the experiment; that is, there should be no physical/chemical interaction between the liquid and solid.
4. The liquid surface tension of the test liquids should be higher than that anticipated from the solid surface tension (ie. $\gamma_{lv} > \gamma_{sv}$).
5. The values of γ_{sv} are assumed to be constant, ie. independent of the liquids used.

Because contact angles have been shown to be a complex phenomena [6, 12, 25, 26], it is advantageous to have a surface where some of these complexities (surface roughness and chemical inhomogeneity) are reduced or eliminated. In other words an ‘ideal’ Young’s surface would be highly desirable. Hence, if a chemically ‘controllable’ interface can be constructed where the effects of surface

roughness and chemical inhomogeneity can be minimized (or eliminated), it is of great interest in enabling further fundamental research on Young's equation (Eq.(1.1)), possibly enabling us to better understand the microscopic phenomena that lead to this macroscopic relation.

One possible system for constructing such an 'ideal' surface are self-assembled monolayers (SAMs) since they modify the surface interfacial properties in a very systematic and controllable way [27, 28]. SAMs are two-dimensional organic assemblies that form via the spontaneous adsorption of molecules onto metal or metal oxide supports. One of the more popular self-assembly systems in literature is that of *n*-alkanethiols $[\text{SH}(\text{CH}_2)_{n-1}\text{CH}_3]$ chemisorbed onto a gold, typically Au(111), substrate [27, 29]. These molecules consist of a methylene (CH_2) 'backbone' with a sulphur atom at one end which forms a stable Au-S bond on the Au substrate. The other end of these molecules consists of a functional tail group which can be modified to obtain different surface properties [27, 28]. These molecules have a strong van-der Waals attraction between the CH_2 backbone chains which yields a stable molecular film on the Au substrate [27, 28]. These systems have been very well characterized and there exists a relatively large body of data in regards to their formation kinetics and ultimate crystalline structure. Therefore, in this thesis, the focus is on these monolayers although the results that will be presented here are applicable to other SAM systems.

Typically these alkanethiol SAMs are thought of as a smooth interface since consist mainly of *all-trans* zig-zag chains with few *gauche* defects present [28, 29], although relative disorder may exist on the methyl surface [27]. How-

ever contact angle studies on these surfaces present a puzzling picture which demands further investigation: the advancing contact angle obtained for a methyl (CH_3) terminated alkanethiol is not what is expected for a CH_3 surface. To explore why this may be the case, this study examined three types of Au substrates — evaporated, annealed, and template-stripped — with differing levels of microscopic roughness together with alkanethiol SAMs (specifically octadecanethiol and dodecanethiol). The bare Au substrates were examined by AFM to characterize the substrate roughness. The adsorbed monolayers were characterized with spectroscopic ellipsometry, FT-IR, and low-rate dynamic contact angle studies. Finally, a model is proposed to explain the experimental data and the suitability of SAMs in studying Eq.(1.1) is confirmed with the construction of a ‘near-perfect’ Young’s surface.

CHAPTER 2

LITERATURE REVIEW

2.1 SAMs on Evaporated Surfaces

2.1.1 History

SAMs origins can be traced to an early paper of Zisman *et. al* [30] where glass surfaces were exposed to dilute solutions of long-chained alcohols in hexadecane and oriented monolayer films were formed on the part of the substrate not wetted by the solvent. Zisman *et. al* continued with various surfactant-like molecules including long-chained amines, carboxylic acids and amides on metal and metal oxide surfaces [31, 32]. However, these systems exhibit only modest stabilities and were limited to low-energy hydrophobic surfaces. Allara *et al.* extended Zisman's work by relying on a stronger Au-S bond for molecular self-assembly [1, 33–35]. The S interaction also allows adsorption of thiols onto other metals such as Ag, Cu, Hg, Pd, GaAs, and InP. This specific S-metal interaction is stronger than the physisorbed molecular Langmuir-Blodgett (LB) films. SAMs have been extensively investigated due to their potential uses as corrosion inhibitors, resist layers, chemical sensors, and models for organic and biological surfaces [27–29]; in part due to the fact that they can be modified chemically at their surfaces for different terminal functional groups. A schematic

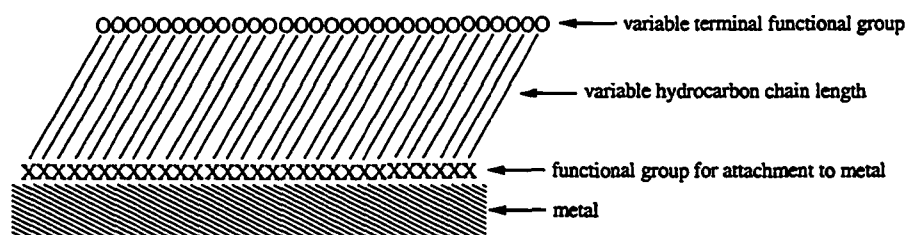


Figure 2.1: Schematic of a typical self-assembled organic monolayer adsorbed onto a metal substrate.

illustrating a typical SAM is shown in Fig.2.1 where the end functional group (sulphur) for attachment to the metal surface is the only part of the molecule which prefers to attach to the metal (hence the self-assembly).

2.1.2 Alkanethiol SAMs

One of the more popular self-assembly systems in the literature is that of alkanethiols chemisorbed onto an Au(111) substrate [27–29]. The structure of the CH_2 backbone chain is shown schematically in Fig.2.2. The molecule's position can be completely described by three angles: the tilt angle with respect to the surface normal θ , the twist angle with respect to rotation about the molecular axis Ψ , and the projected angle in the x - y plane α . The molecule is considered fully extended if *gauche* defects are not considered [29]. For the simple model used in this thesis, the only angle considered is the tilt angle θ . Typical reported values for θ , Ψ and α in literature for alkanethiols (where $n \geq 12$) adsorbed onto Au(111) are $\sim 30^\circ$ [1, 2, 27–29], $\sim 55^\circ$ [2, 27, 29], and $\sim 8^\circ$ [29] respectively. The monolayer molecules are believed to be *all-trans* zig-zag chains with few *gauche* defects present [28, 29], although relative disorder may exist on the functional

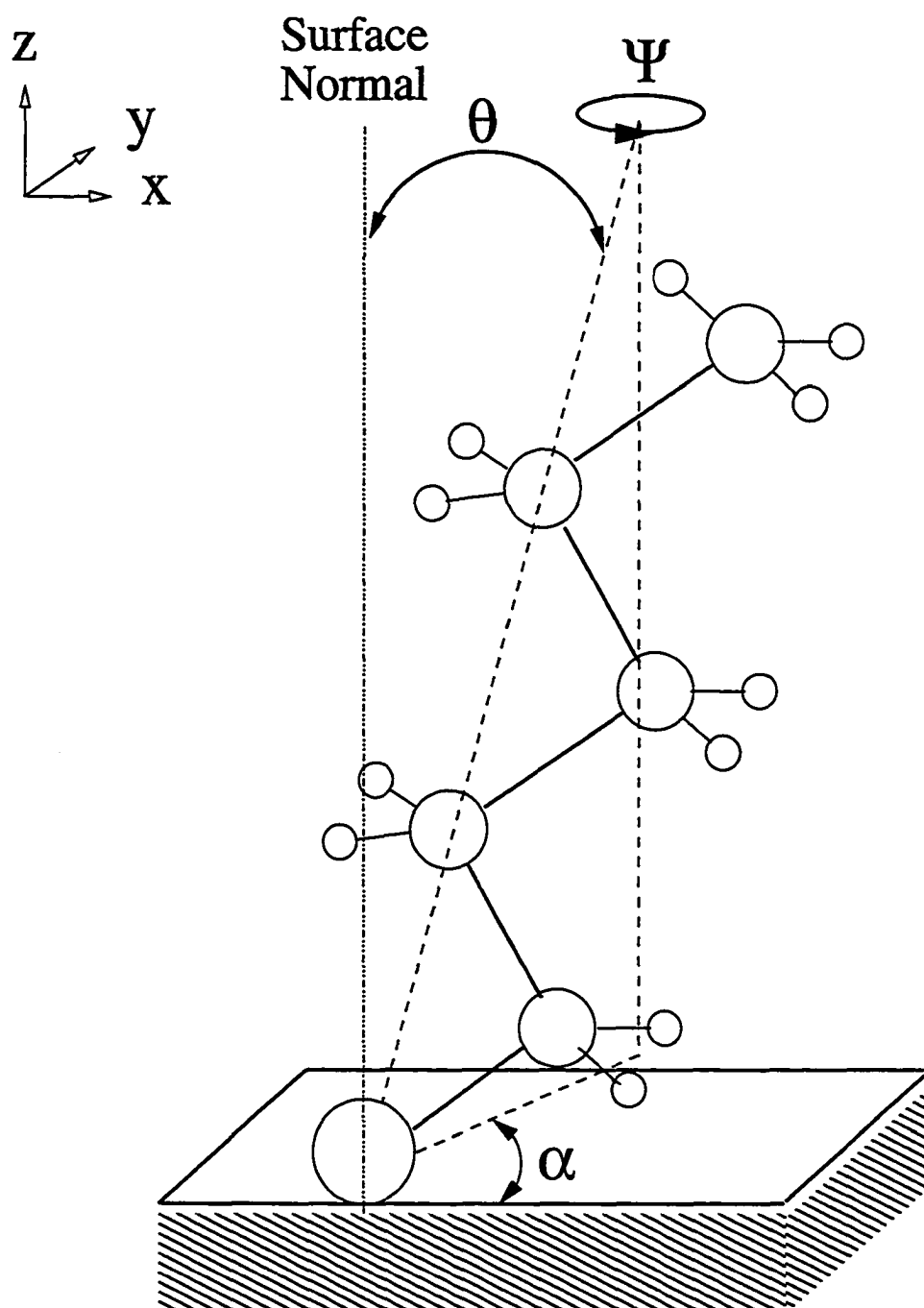


Figure 2.2: Schematic of the alkanethiol molecule adsorbed on Au. In this case, the terminal functional group shown is the methyl (CH_3) molecule.

terminal-group surface [27].

SAMs form spontaneously by immersion into an organic solution with concentrations in the micromolar to millimolar range [27, 29]. Kinetic studies of the adsorption mechanism of the alkanethiols onto the Au substrate have shown a two-step (or even three) adsorption process with a fast step (minutes) achieving 80-90% of the final monolayer coverage and a slower step (hours) which takes many hours for completion [10, 27, 36–38]. Thus it is critical to ensure that enough time is allowed for complete monolayer formation.

The substrate that the monolayer forms on is also of interest since the final monolayer configuration is dependent upon the metal's crystallization as has been shown in several studies [2, 3, 11, 27–29, 39, 40]: on different metal substrates, monolayer formation yields different final configurations.

2.1.3 Atomic Force Microscopy (AFM)

The typical Au(111) substrate that the SAM is adsorbed onto is an evaporated Au surface on a Si(100) wafer with a Ti (titanium) or Cr (chromium) adhesion layer. In the literature such an Au substrate examined by Atomic Force Microscopy (AFM) or Scanning Tunneling Microscopy (STM) yields peak to valley (PV) roughness values of 8-15nm and an average terrace size of 25-50nm depending upon the evaporation rate used [41–45].

2.1.4 Spectroscopic Ellipsometry

At first, in the literature, the ellipsometry measurement of alkanethiol monolayer thickness was performed with a single wavelength ellipsometer at a wavelength of 632.8nm [1, 3, 10, 33, 35, 46–57]. Thus, only one set of values were necessary

for the optical constants and the values typically chosen for alkanethiols were $n=1.45$ (or 1.46, 1.50) and $k=0$ [1, 3, 10, 33, 35, 46–57]. Measurements are usually taken at a 70 or 75° angle from the surface (i.e. 10 or 15° from surface normal).

The ellipsometric thicknesses reported in the literature for alkanethiol monolayers is ~ 1.5 Å per CH₂ molecule (if the number of CH₂ > 10) [1, 3, 10] and a lower slope when the number of CH₂ are < 10. These different regimes can be clearly seen in Fig.2.3; the cut-off to different regimes appears to be ~ 7 CH₂ molecules.

For alkanethiols the theoretical thickness of a fully extended *all-trans* chain is expected to be a 4 Å intercept plus 1.27 Å/CH₂ [10], i.e.

$$t = 4 + 1.27n \quad (2.1)$$

where t is the monolayer thickness (in Å) and n is the number of CH₂ molecules in the alkanethiol backbone. Thus, for a fully extended *all-trans* octadecanethiol monolayer the thickness is calculated by Eq.(2.1) to be ~ 25.6 Å; hence an octadecanethiol monolayer tilted at an average of 30° would be expected to be 22.2 Å thick. For dodecanethiol, the fully extended *all-trans* monolayer would therefore be 19.2 Å and a 30° average tilt would yield a thickness of 16.7 Å.

2.1.5 Fourier Transform Infrared (FT-IR)

Porter et. al [1] first assigned the typical C-H stretching modes for alkanethiol molecules; these assignments are reproduced in Table 2.1 as well as part of their experimental results which are typical of literature Fourier Transform Infrared (FT-IR) results for alkanethiol monolayers. These orientations were further

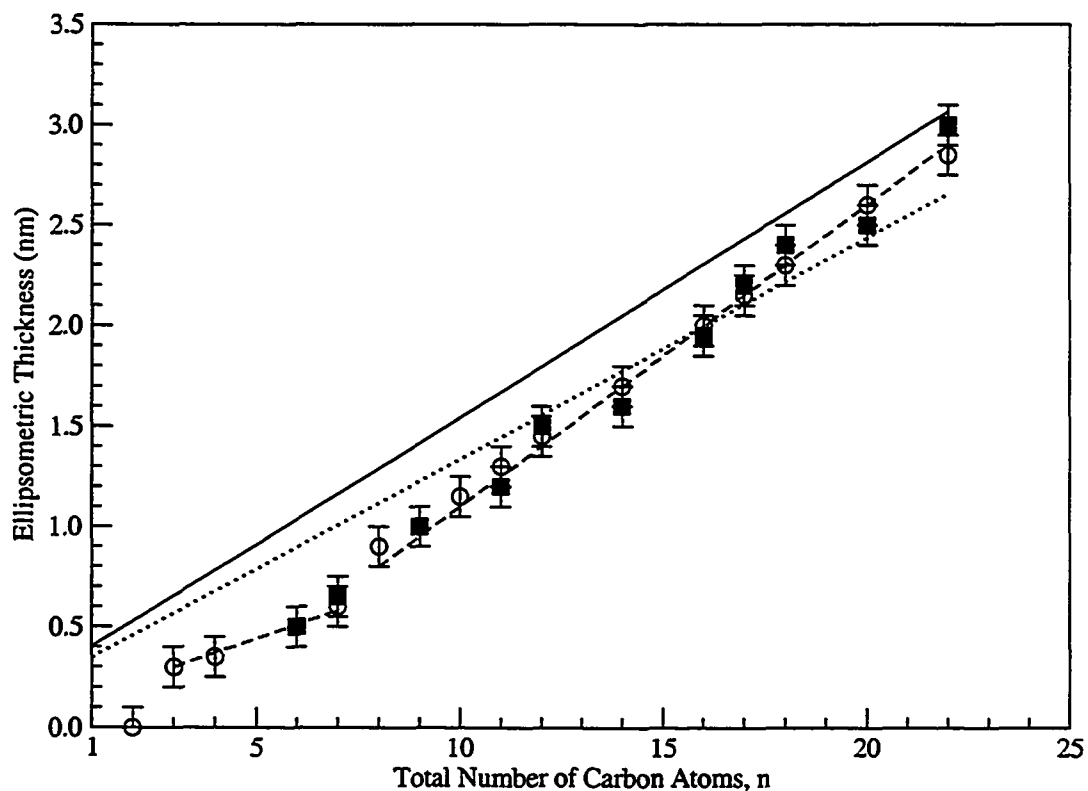


Figure 2.3: Ellipsometric thicknesses reported for $\text{SH}(\text{CH}_2)_{n-1}\text{CH}_3$ (alkanethiols) in [9] (■, as an estimated average thickness) and [10] (○, as an estimated thickness). The solid line represents the limiting case of a fully extended *all-trans* molecule (calculated by Eq.(2.1)) and the dotted line is the monolayer at a 30° tilt. The dashed line is provided as an aid to the eye to estimate the slope of the experimental data. Error bars (± 0.1 nm) are due to estimation of thicknesses from figures in [9, 10].

elucidated by Laibinis et. al [2]. The peak position clearly shifts from a crystalline state (in KBr) to the liquid state; this helps in inferring the relative order/disorder of the monolayer adsorbed onto Au — if the peak is shifted towards the liquid position it is “liquid-like”, meaning relatively disordered. The widths and intensities of the peak also yield useful information regarding monolayer structure: tightly banded peaks are consistent with a crystalline-like environment [35, 57], thus a widening in the peak is suggestive of increasing ‘disorder’ in the monolayer.

Table 2.1: Peak positions for $\text{SH}(\text{CH}_2)_{n-1}\text{CH}_3$ C-H stretching modes for crystalline state, liquid state and adsorbed onto Au substrate and the assigned direction of the transition dipole (reproduced from [1, 2]). Note that n = total number of carbon atoms in the molecule.

C-H stretching mode ^b	assigned dir. of transition dipole ^c	peak positions ^a (cm^{-1})					
		in KBr $n=22^d$	liq. $n=8^e$	adsorbed on Au $n=22$ $n=18$ $n=12$ $n=6$			
$\nu_a(\text{CH}_2)$	\perp CCC backbone plane	2918	2924	2918	2917	2919	2921
$\nu_s(\text{CH}_2)$	ip CCC backbone plane,	2851	2855	2850	2850	2851	2852
$\nu_a(\text{ip})(\text{CH}_3)$	ip HCH plane ip CCC backbone, \perp C-CH ₃ bond	<i>f</i>	<i>f</i>	2965	2965	2965	2966
$\nu_a(\text{op})(\text{CH}_3)$	\perp CCC backbone plane	2956	2957	<i>g</i>	<i>g</i>	<i>g</i>	<i>g</i>
$\nu_s(\text{FR})(\text{CH}_3)$	\parallel C-CH ₃ bond	<i>h</i>	<i>h</i>	2937	2938	2937	2939
$\nu_s(\text{CH}_3)$	\parallel C-CH ₃ bond	<i>h</i>	<i>h</i>	2879	2878	2879	2878

^a peak positions are an average of 4 independent spectra and accurate within 1cm^{-1}

^b vibration mode: ν_a asymmetric stretch, ν_s symmetric stretch, (ip) in-plane, (op) out-of-plane, (FR) Fermi resonance

^c \perp perpendicular, \parallel parallel, ip in-plane, op out-of-plane

^d crystalline, $\text{SH}(\text{CH}_2)_{21}\text{CH}_3$ in KBr

^e liquid, $\text{SH}(\text{CH}_2)_7\text{CH}_3$ in liquid prism cell

^f the $\nu_a(\text{ip})$ is masked by the strong $\nu_a(\text{op})$

^g the position for $\nu_a(\text{op})$ cannot be determined due to low signal-to-noise ratio. This is a result of the orientation of this mode with respect to the surface.

^h both $\nu_s(\text{FR})$ bands are masked by the $\nu_a(\text{CH}_2)$ band.

2.1.6 Advancing Contact Angle

The contact angle method typically used is a drop deposited on the surface with the needle still in contact with the drop from above and the angle measurements are made with a goniometer which has an accuracy of $\pm 2^\circ$ [12].

The literature on alkanethiols usually reports a decrease in advancing contact angle θ_a , with a decrease in the CH_2 chain length. This decrease often starts somewhere around when the number of carbon atoms in the molecule is less than 12 as seen in Fig.2.4.

There are problems with the use of the goniometer in measuring contact angles — other than the accuracy of the device. It has been shown [6, 12, 16, 25] that using a goniometer to measure the contact angle can produce the actual advancing angle but often misses the complexity of the contact angle behavior and hence one of the following conditions are (inadvertently) violated:

1. there can be no slip/stick movement of the three phase contact line,
2. the contact angle cannot increase/decrease as the drop front advances,
and
3. the liquid surface tension cannot change as the drop front advances.

Since the goniometer technique may miss these conditions the contact angles given in the literature need to be used with caution; especially since at least one study [12] has produced non-constant γ_{lv} and θ_a for octadecanethiol adsorbed on an Au substrate - violating the conditions given above. Therefore, the contact angles given for alkanethiol SAMs in the literature are to be approached with caution.

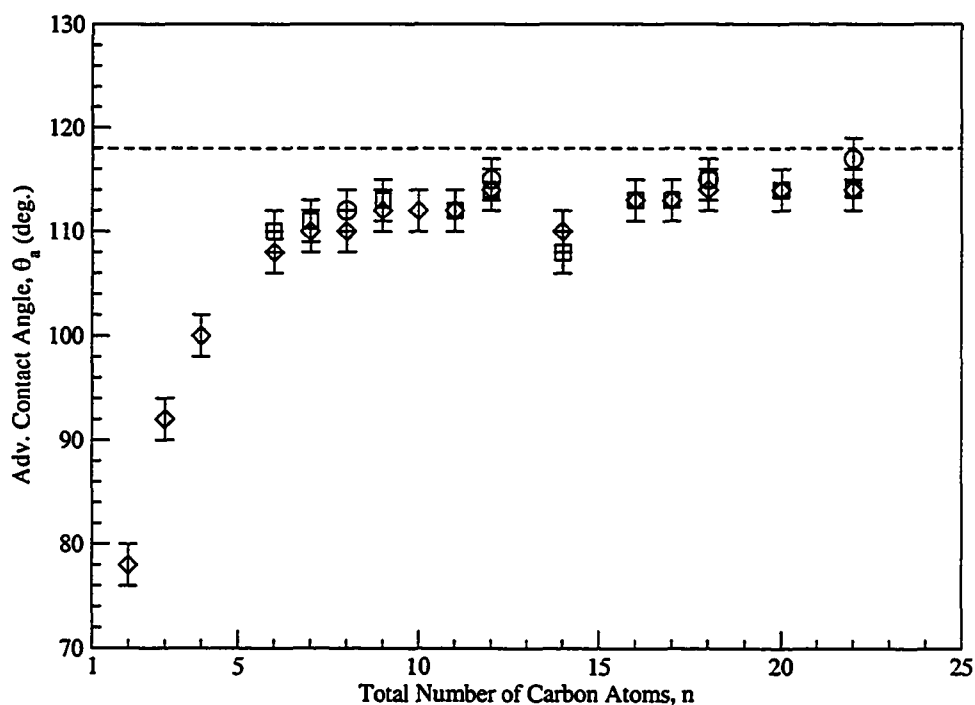


Figure 2.4: Typical curve for advancing contact angles of water on alkanethiols adsorbed on Au reported in literature for the different chain lengths, $\text{SH}(\text{CH}_2)_{n-1}\text{CH}_3$. Plotted values (\circ) come from [4], (\square) from [9] and (\diamond , method B where possible) from [10]. The dotted line is \sim the highest reported contact angle on a methyl (CH_3) terminated surface ([5, 11] and results shown here). The error bars ($\pm 2^\circ$) are due to the goniometer error [12]. Note the quoted reproducibility in [4] is $\pm 3^\circ$.

2.1.7 Contact Angle Hysteresis

Recalling the above caution regarding contact angles, the contact angle hysteresis reported in literature for alkanethiol SAMs is now examined. Contact angle hysteresis (H) is defined as:

$$H = \theta_a - \theta_r \quad (2.2)$$

where θ_a is the advancing contact angle and θ_r is the receding contact angle. Hysteresis is attributed to several factors in literature: surface roughness [58–64], chemical inhomogeneity of the surface [65–72], and molecular mobility and packing [73–75]. These causes can be described in terms of metastable states; recent studies have focused on ‘true’ hysteresis in the sense of liquid penetration and surface swelling [64, 76, 77], or even in terms of liquid retention [64]. Thus, contact angle hysteresis in general is suggestive of surface quality [11].

Examining the receding contact angles θ_r given in literature for alkanethiols adsorbed on an Au substrate (with a corresponding θ_a) [2–5] and applying Eq.(2.2), Table 2.2 was generated. From this table, it is immediately apparent that there are variations in the contact angle hysteresis which is consistent with literature results for contact angles in general — not just for alkanethiols.

2.1.8 Contact Angle Interpretation

A large body of work [6–8, 11, 16, 25, 26, 78–84] has shown that experimental contact angles on a large number of polymer surfaces yield smooth curves for $\gamma_{lv} \cos \theta$ versus γ_{lv} , $\cos \theta$ versus γ_{lv} , and W_{sl} versus γ_{lv} for one and the same solid surface. Changing the solid surface simply shifts the curve in a regular manner as shown in Fig.2.5 which suggests that the following relations exist:

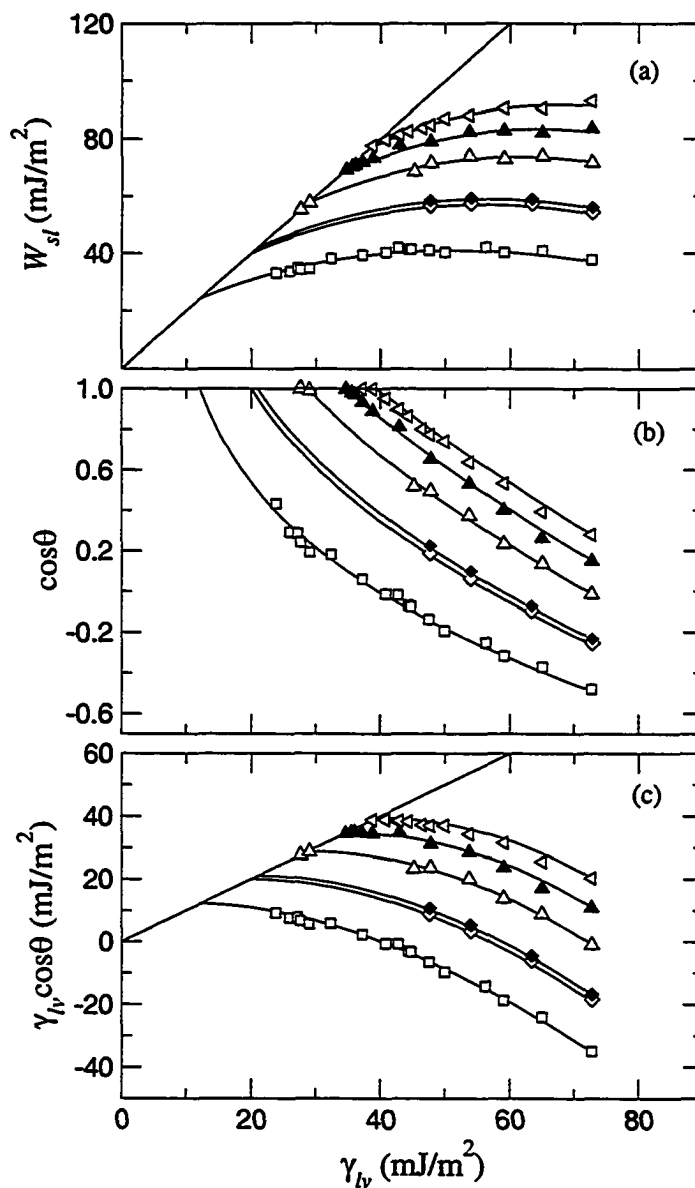


Figure 2.5: (a) The solid-liquid work of adhesion W_{sl} , (b) the cosine of the contact angle, $\cos\theta$, and (c) the liquid-vapor surface tension times the cosine of the contact angle, $\gamma_{lv} \cos\theta$, versus the liquid vapor surface tension, γ_{lv} . Data shown for fluorocarbon FC722 (\square), hexatriacontane (\diamond), cholesteryl acetate (\blacklozenge), poly(*n*-butyl methacrylate) (\triangle), poly(methyl methacrylate/*n*-butyl methacrylate) (\blacktriangle), and poly(methyl methacrylate) (\triangleleft) surfaces

Table 2.2: Contact angle hysteresis (H) in degrees ($^{\circ}$) for $\text{SH}(\text{CH}_2)_{n-1}\text{CH}_3$ adsorbed onto Au for water (H_2O) and hexadecane (HD). Data from [2-5]^a.

n	Laibinis et. al [2]		Jennings et. al [3]		Laibinis, Whitesides [4]		Sondag-Huethorst et. al [5]	
	H_2O	HD	H_2O	HD	H_2O	HD	H_2O	HD
6	13	11						
7	14	10						
8	14	12			9	11		
9	14	11						
10	12	12						
11	12	13						
12	12	12			11	13	14	15
14	9	9						
15	12	10						
16	10	9						
17	14	12						
18	10	12	9	5	10	12	27	20
19	10	10						
20	10	10						
22	12	11			17	9	29	21

^a data from [2] estimated from figures (error at least $\pm 2^{\circ}$). All refs. measured contact angles with goniometer (accuracy $\pm 2^{\circ}$). Blank spaces are left where data was not available.

$$\gamma_{lv} \cos \theta = f_1(\gamma_{lv}, \gamma_{sv}) \quad (2.3)$$

$$\cos \theta = f_2(\gamma_{lv}, \gamma_{sv}) \quad (2.4)$$

and

$$W_{sl} = f_3(\gamma_{lv}, \gamma_{sv}) \quad (2.5)$$

The adhesion and contact angle patterns reproduced in Fig.2.5 for the six surfaces (fluorocarbon FC722 [6], hexatriacontane [12, 13, 85, 86], poly(*n*-butyl methacrylate) [8], poly(methyl methacrylate/*n*-butyl methacrylate) [87], and

poly(methyl methacrylate) [78]) in addition to other results suggest the existence of universal patterns for low-energy solid surfaces. If a polymer with predominantly methyl (CH_3) groups exposed to the surface is chosen to compare with the CH_3 terminated alkanethiol monolayers, it is expected that both the polymer and the monolayers would fall on the same curve as they both are expected to have CH_3 surfaces. For this purpose, hexatriacontane was chosen as a basis for comparison as it has a predominantly CH_3 surface and the quality of the hexatriacontane surface prepared by vapor deposition was so good that no contact angle hysteresis for water was observed [13]. If the literature values for advancing contact angles for hexatriacontane are compared with those for CH_3 terminated alkanethiols in the form of Fig.2.5 (shown in Fig.2.6) it is clear that the monolayer data exhibits considerable scatter from the hexatriacontane. The question then becomes: is this scatter due to some fundamental difference between monolayers and polymers or is there some other reason(s) which complicate the picture given here?

2.2 Flat substrates

2.2.1 Ultraflat Template-stripped Surfaces

Recently, in the literature, a new method of producing ultra-flat surfaces has emerged; that of template-stripping. In this procedure, a metal that is going to be used as the monolayer substrate is evaporated onto Si or mica and then either mica, Si or glass is glued to the metal which is then "stripped" from the surface [45, 88–94]. This freshly "stripped" surface can be immediately immersed in the SAM solution thus avoiding problems with atmospheric contamination of the

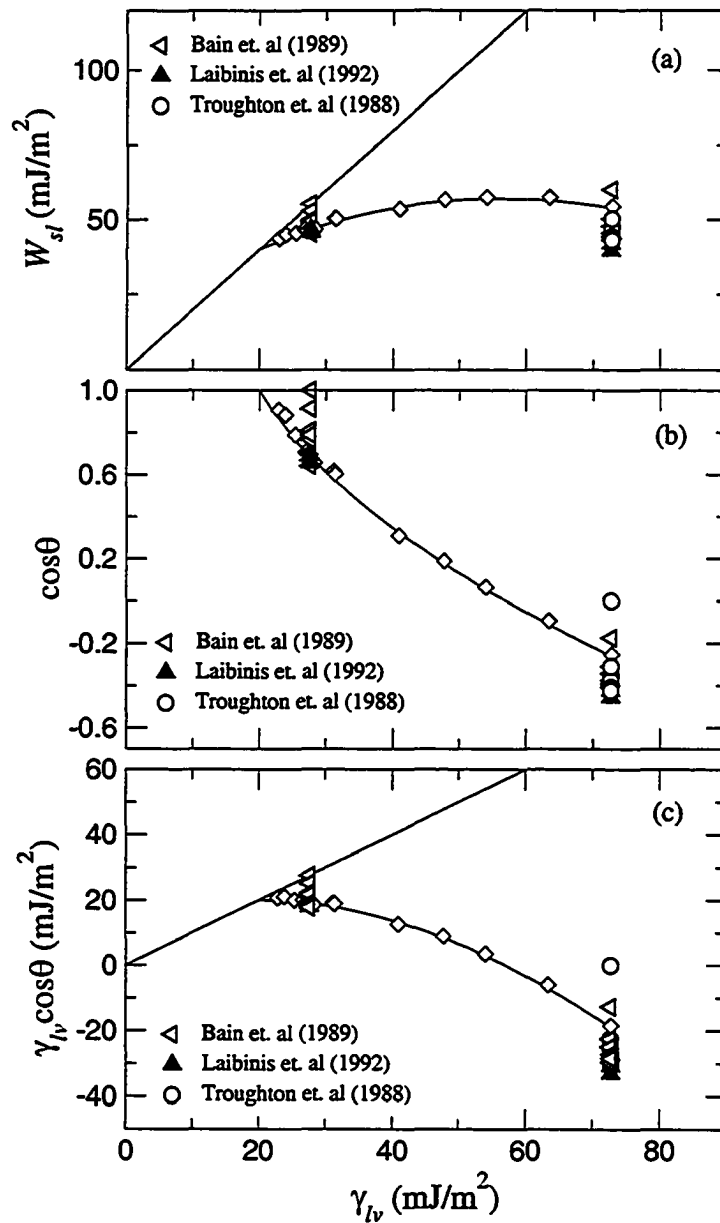


Figure 2.6: A comparison of the CH_3 terminated polymer hexatriacontane (\diamond [13]) with literature data for CH_3 terminated alkanethiols (\triangleleft [10], \circ [9], and \blacktriangle [4]). (a) The solid-liquid work of adhesion W_{sl} , (b) the cosine of the contact angle, $\cos\theta$, and (c) the liquid-vapor surface tension times the cosine of the contact angle, $\gamma_{lv} \cos\theta$, versus the liquid vapor surface tension, γ_{lv} .

metal substrate prior to the monolayer formation. These surfaces exhibit very small peak-to-valley and root-mean-square (*rms*) roughness values relative to annealed and especially evaporated surfaces; they are microscopically flat over relatively large areas.

There are some difficulties with “stripping” from mica as the force required is large [90] and can induce undesirable stresses. Recently Ulman et. al [94] reported that the Au coated mica with the glass glued to it can be immersed directly in the SAM solution which then releases the metal (the solution is of a solvent type reported in [89]) from the mica and coats the metal with the SAM simultaneously.

CHAPTER 3

EXPERIMENTAL SETUP

3.1 Materials

Test grade silicon (Si) wafers (100 orientation) were obtained from Wafer World (West Palm Beach, FL) in 100 mm diameter discs. Au (99.999%) and titanium (Ti, 99.995%) shots were obtained from Kurt J. Lesker (Clairton, PA). Ethanol (100%) was obtained from the chemistry dept. at the University of Alberta. Methanol (100%), octadecanethiol [$\text{CH}_3(\text{CH}_2)_{17}\text{SH}$] and dodecanethiol [$\text{CH}_3(\text{CH}_2)_{11}\text{SH}$] were obtained from Aldrich and used as received.

The liquids chosen for contact angle measurements were selected based on the following criteria [17, 19, 95, 96]:

1. they should include a wide range of intermolecular forces;
2. they should be non-toxic; and
3. the liquid surface tension should be higher than the anticipated solid surface tension ($\gamma_{lv} > \gamma_{sv}$).

The chosen liquids are listed in Table 3.1 along with their experimentally determined liquid-vapor surface tension (γ_{lv}) from previous studies [6–8]. DIUF

Table 3.1: Experimental liquid-vapor surface tensions^a determined via pendant drop method (ADSA-P) [6–8]

liquid	γ_{lv} (mJ/m ²)
water	72.70 \pm 0.09
formamide	59.08 \pm 0.01
ethylene glycol	47.55 \pm 0.02
bromonaphthalene	44.31 \pm 0.05
decanol	28.99 \pm 0.01
hexadecane	27.62 \pm 0.01

^a \pm values are the 95 % confidence limits.

(de-ionized ultra-filtered) water was obtained from Fisher Scientific (Ontario, Canada) and used as received. Hexadecane (99+%, anhydrous), 1-bromonaphthalene (97%), decanol (decyl alcohol, 99%), formamide (99.5+%), and ethylene glycol (99+%) were obtained from Aldrich and used as received.

The epoxy (EPO-TEK 377) was obtained from Epoxy Technologies (MA) and used as received. EPO-TEK 377 is a two part epoxy that contains no solvent and is resistant to many organic solvents such as the alcohols typically used in the deposition of self-assembled monolayers. EPO-TEK 377 is heat activated and requires at least 1 hour at 150°C to cure.

Standard 100 mm \times 25 mm glass microscope slides were obtained from Fisher Scientific (Ontario, Canada) and 1 mm diameter holes were drilled into pieces of glass (at least 25 mm square) using a 1 mm diamond bit (SMS-0.027) from Lunzer (New York, NY.).

3.2 Preparation of Evaporated and Annealed SAMs.

The Si wafer was cut into small into rectangular shapes of about $2.5 \text{ cm} \times 5 \text{ cm}$. These Si pieces were then drilled with a $\sim 1 \text{ mm}$ bit and thoroughly rinsed with ethanol before the Au and Ti were evaporated onto the Si. Samples used for AFM studies were evaporated onto $\sim 1 \text{ cm}^2$ (non-drilled) Si samples.

The Au substrates were prepared by sequentially evaporating Ti ($\sim 10 \text{ nm}$) and Au ($\sim 100 \text{ nm}$) onto small rectangular silicon wafers in a diffusion-pumped vacuum chamber at $\sim 10^{-6}$ torr. The chamber was backfilled with air and the substrates were used within 48 h of preparation. The evaporated surfaces were rinsed with ethanol before SAMs formation. SAMs were prepared by immersing the Au surfaces into 1 mM of $\text{CH}_3(\text{CH}_2)_{17}\text{SH}$ in ethanol overnight. The resulting surfaces were thoroughly rinsed with ethanol and blown dry by nitrogen (N_2) gas before use.

Evaporated gold substrates were also flame annealed for $\sim 30 \text{ s}$ using a bunsen burner under ambient laboratory condition. After ~ 1 minute, the annealed substrate was then immersed into 1 mM of $\text{CH}_3(\text{CH}_2)_{17}\text{SH}$ in ethanol overnight.

3.3 Preparation of Template-Stripped SAMs.

Au films were prepared by evaporating Au ($\sim 100 \text{ nm}$) at $\leq 0.2 \text{ nm/s}$ onto freshly 'clean' silicon wafers in a diffusion-pumped vacuum chamber at $\approx 2 \times 10^{-6}$ torr. The chamber was backfilled with air and the substrates were used within 24 h of preparation. The two-part epoxy (EPO-TEK377) was mixed at 1:1 weight ratio and applied carefully to the drilled glass pieces which were then

placed on the evaporated Au surface. It is critical that air bubbles be eliminated from the glue before applying it to the surface. Any bubbles that are present before putting the samples into the oven translate into defects where the gold does not attach to the glass. Several samples were forced to be discarded due to defects of this nature. Samples used for AFM studies were glued to $\sim 1 \text{ cm}^2$ (non-drilled) glass samples.

The epoxy was then cured by placing the wafers in an oven for at least 1 h at 150°C . The wafers were then removed from the oven and allowed to cool. Once cured, the wafers were placed on a shelf for storage until samples were needed. Previous studies have found no differences between samples stripped immediately after curing the epoxy and those stripped after sitting on the shelf for a period up to 2 months [45].

To ‘strip’ a fresh sample from the wafer, a razor blade was used. First the sharp razor blade was run around the edge of the sample to separate the sample from excess epoxy on the surface. Then, the tip of the blade was gently pushed under one corner of a sample and used to pry the sample up. Extreme care must be taken in removing the glass; several samples were ruined during this process and had to be discarded.

To minimize contamination, all template-stripped samples were **immediately** immersed into solution upon removal from the silicon wafer (exposure to atmosphere $< 30 \text{ s}$) to minimize atmospheric contamination of the Au substrate. Octadecanethiol SAMs were prepared by immersing the stripped samples in 5 mM of $\text{CH}_3(\text{CH}_2)_{17}\text{SH}$ in ethanol overnight. Dodecanethiol SAMs were prepared by immersing the stripped samples in 2 mM of $\text{CH}_3(\text{CH}_2)_{17}\text{SH}$ in

methanol overnight. The resulting surfaces were rinsed thoroughly with ethanol and blown dry by N₂ gas before use.

3.4 Characterization of SAMs.

3.4.1 AFM — Evaporated and Annealed Samples

The atomic force microscopy (AFM) measurements were performed using a Digital Instruments Nanoscope IIIa atomic force microscope (Digital Instruments, Santa Barbara, CA). Commercial silicon nitride cantilevered probes were used with a force/spring constant in the range between 0.06 – 0.58 N/m. The AFM images of annealed and evaporated Au surfaces were captured by using contact mode under ambient laboratory conditions.

3.4.2 AFM — Template Stripped Samples

The AFM measurements were carried out in contact mode under ambient conditions using commercial Si₃N₄ cantilevers (ThermoMicroscope) with a force/spring constant in the range between 0.05-0.5 N/m and a radius of curvature ≤ 20 nm. Digital Instruments Multi-mode and Dimension 3000 microscopes were used to perform the measurements. For the root-mean-square (*rms*) and peak-to-valley (PV) roughness values, several scans at random locations across at least two different samples were taken and the Digital Instruments software was used to determine the roughness of each scan (a first order flattening followed by the roughness calculations). The independent values were then averaged and the standard deviation taken as an estimate of the error on the quoted values.

3.4.3 Spectroscopic Ellipsometry

The prepared SAMs were first characterized by a Sopra GESP5 Variable Angle Spectroscopic Ellipsometer. The ellipsometry measurements were performed using a rotating polarizer in the current tracking analyzer mode. The measurements were taken over a wavelength range of 300 – 850 nm at 20 nm intervals. The linearly polarized light was directed onto the film surface at an incident angle of 75° from the surface normal. Immediately after stripping, $\tan\Psi$ and $\cos\Delta$ for each bare Au substrate were measured as references. After immersion of the substrates into the octadecanethiol/ethanol (or dodecanethiol/methanol) solution overnight, a new set of $\tan\Psi$ and $\cos\Delta$ for each sample were measured. An ambient/thin-film/substrate model was constructed where:

1. the ambient was set to air ($n = 1$, $k = 0$ for all λ);
2. the thin-film was set to a crystalline CH_3 terminated -thiol monolayer adsorbed onto Au ($n = n(\lambda)$, $k \cong 0$) which was obtained independently from Sopra, rather than assuming an index of refraction (e.g. $n = 1.46$) as is typically done in the literature [1, 3, 10, 33, 35, 46–57];
3. the substrate was set to Au, i.e. a calculated refractive index from the bare Au reference measurement (calculated with $t = \infty$).

This model was used for regression to fit the measured curve by varying the thin film model thickness t which was calculated according to the following equation:

$$(\tan\Psi) e^{(i\Delta)} = f(n_j(\lambda), k_j(\lambda), t_j) \quad (3.1)$$

where the subscript j represents each layer, $n(\lambda)$ and $k(\lambda)$ are the optical constants of each layer, and t is each layer's thickness ($t_{\text{substrate}} = \infty$ and $t_{\text{thin film}} = x$, where x is some reasonable initial guess for the thin film thickness).

3.4.4 FT-IR

Reflectance infrared (IR) spectra of the -thiol SAMs on Au were obtained using a ThermoNicolet Nexus 670 spectrometer equipped with a VeeMax grazing angle accessory. The IR light was incident at 75° normal to the surface and the reflected light was passed through a polarizer [97] to a MCT-A (mercury-cadmium-telluride) liquid N₂ cooled detector. The spectra resolution was 0.964 cm⁻¹ and the IR aperture was kept constant at 32 which corresponds to ≈ 0.16 cm² IR aperture area. Spectra were referenced to the corresponding bare Au substrates and 512 scans were obtained for good signal-to-noise ratios. An infrared gain of 4 was selected for all reflectance IR measurements to ensure that the input IR signals were constant. All spectra presented in this thesis have been baseline corrected for clarity.

The liquid spectra used in this thesis were obtained via an ATR (attenuated total reflection) accessory (Nicolet ARK) with a KBr (potassium bromide) trough with the KBr crystal cut at 40°. All spectra were obtained with 256 scans and at a resolution of 0.482 cm⁻¹ with the IR aperture set to 32 and a gain of 1 for all ATR measurements. A background spectra was taken of the empty trough and then spectra were obtained for the ethanol, methanol and the SAM solutions, respectively. The ethanol/methanol spectra were then subtracted from the solution spectra to obtain the octadecanethiol/ dodecanethiol spectra. In this way, the effect of the ethanol and/or methanol can be eliminated

since their signal is \gg than that of either the octadecanethiol or dodecanethiol and completely obscures their contribution to the collected spectra.

3.4.5 Contact Angle Measurements

Contact angle measurements were chosen as the last step for the characterization of SAMs. A Linux version of the Axisymmetric drop shape analysis - profile (ADSA-P) was used for sessile drop contact angle measurements. ADSA-P is a technique to determine liquid-fluid interfacial tensions and contact angles from the shape of axisymmetric menisci, i.e., from sessile as well as pendant drops [98, 99]. Assuming that the experimental drop is Laplacian and axisymmetric, ADSA-P finds a theoretical profile that best matches the drop profile extracted from an image of a real drop, from which the surface tension, contact angle, drop volume, surface area and three-phase contact radius can be computed. The strategy employed is to fit the shape of an experimental drop to a theoretical drop profile according to the Laplace equation of capillarity, using surface/interfacial tension as an adjustable parameter. The best fit identifies the correct surface/interfacial tension from which the contact angle can be determined by a numerical integration of the Laplace equation. To collect the data to be analyzed by ADSA-P, the set-up shown in Fig.3.1 was used. The needle that passes through the sample is carefully wrapped with Teflon tape to ensure that liquid does not pass back through the table or sample hole. The sessile drop setup must be levelled and is on a vibration free table to ensure that accurate contact angles are measured since no vibrations are passed to the liquid. The needle and fittings were carefully cleaned between each probe liquid; a different teflon tube was used for each liquid to avoid cross contamina-

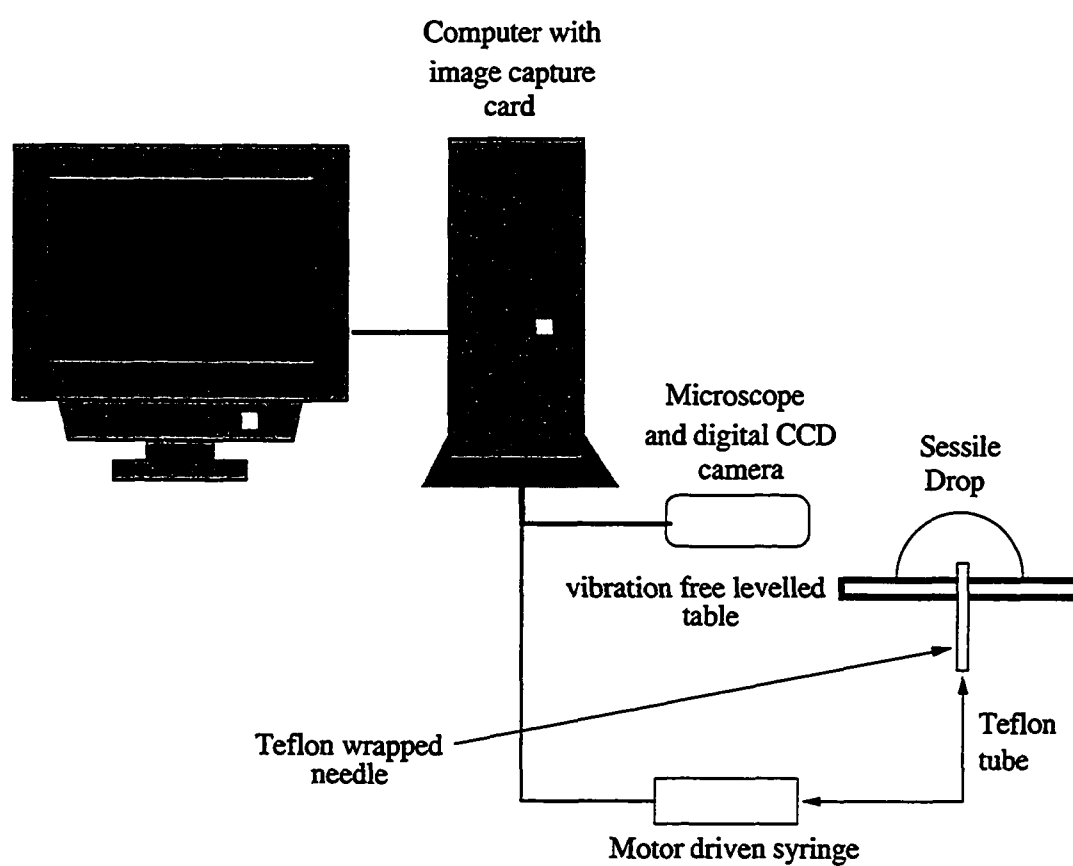


Figure 3.1: Sessile drop experimental setup used to capture images to be analyzed with ADSA-P.

tion of liquids. The cleaning method used was to rinse thoroughly with ethanol and then sonicate (Aquasonic 75D, VWR Scientific Products) for 15 minutes in ethanol before drying with N_2 gas and leaving under a drying lamp if necessary.

To capture the data, a drop of liquid ~ 0.30 cm in radius was placed carefully over the needle to ensure that the drop will increase axisymmetrically when the motorized syringe is used to increase the drop volume from beneath the sample. Pictures were taken \sim every 0.5 seconds and recorded on the computer hard-drive for analysis by ADSA-P. The advancing (θ_a) and receding (θ_r) angles are obtained by increasing/decreasing the drop volume by pushing/pulling on the motorized syringe. This in turn increases/decreases the drop radius and hence moves the three-phase contact line. The computer controlled the rate at which the motorized syringe supplied liquid to the drop; by adjusting the step count, the advancing/receding rate could be controlled. (These procedures can also be found elsewhere [6, 25, 98, 99]).

Sessile drop experiments were performed by ADSA-P to determine the advancing and receding contact angles. The temperature and relative humidity were maintained, respectively, at $23.0 \pm 0.5^\circ\text{C}$ and at about 30%, by means of an air-conditioning unit in the laboratory. It has been found that, since ADSA-P assumes an axisymmetric drop shape, the values of liquid surface tensions measured from sessile drops are very sensitive to even a very small amount of surface imperfection, such as roughness and heterogeneity, while contact angles are less sensitive. Therefore, the liquid surface tensions used in this study were independently measured by applying ADSA-P to a pendant drop, since the axisymmetry of the drop is enforced by using a circular capillary. Results of the

liquid surface tension from previous studies [6–8] are reproduced in Table 3.1.

In order to use low-rate dynamic contact angle measurements using automated axisymmetric drop shape analysis (ADSA), three conditions must not be violated:

1. there should be no slip/stick movement of the three phase contact line,
2. the contact angle cannot increase/decrease as the drop front advances,
and
3. the liquid surface tension cannot change as the drop front advances.

Any contact angles determined from data that violates these three conditions cannot be used to determine solid surface tensions — and indeed are not Young’s contact angles (ie. θ_Y in Eq.(1.1)) [6, 25, 26].

In this study, at least 4 and up to 16 dynamic contact angle measurements at velocities of the three-phase contact line in the range from 0.1 to 1.0 mm/min were performed for each liquid. The choice of this velocity range was based on previous studies [6, 25, 100, 101] which showed that low-rate dynamic contact angles at these velocities — for these relatively smooth surfaces — were essentially identical to the static contact angles. Liquids were supplied from below the surface through a hole of ~ 1 mm in diameter on the substrate by means of a motorized-syringe system. Details of this setup have been described above (see also [6, 18]).

CHAPTER 4

RESULTS

4.1 AFM

4.1.1 Evaporated Au

Examining Fig.4.1, it is clear that the evaporated Au has an average PV roughness of ~ 15 nm [11]. Furthermore, the average plateau size is estimated to be ~ 40 – 50 nm as is seen in Fig.4.1(b). Other studies [40] have reported *rms* roughnesses of 5.9 Å for this type of Au surface.

4.1.2 Annealed Au

The annealed Au plateau sizes are much larger than the original evaporated Au as is seen in Fig.4.2. The average plateau size is estimated to be ~ 150 nm. The PV roughness is still 15 nm as seen by the scale in Fig.4.2.

4.1.3 Template-Stripped Au

The AFM data for template-stripped surfaces in this section was collected by Jason J. Blackstock in a collaborative research effort submitted to Langmuir [102].

Figure 4.3 shows AFM images taken of the template-stripped Au surface

collected immediately after the stripping procedure.

It is clear in examining these figures that the template-stripped Au has terraces that are approximately the same dimension as the plateaus of the evaporated Au, i.e. $\sim 40\text{--}50$ nm (see Fig.4.1(b) for a zoomed in view of the evaporated surface), and far smaller than those of the annealed Au (average ~ 150 nm). The template-stripped Au, on the other hand, is much smoother as seen in Fig.4.3 with a *rms* roughness of $0.23\text{ nm} \pm 0.02\text{ nm}$ and a PV roughness of $1.80\text{ nm} \pm 0.15\text{ nm}$.

4.1.4 Comparison of AFM images for evaporated, annealed, and template-stripped Au samples

Other studies [45, 88, 89, 93] have reported similar roughnesses for template-stripped Au. Recently, Ragan et al. [103] have shown that the steps in the case of single crystal platinum exhibit step ‘bunching’, resulting in multi-atomic step heights between neighboring terraces. It is very likely that this same structure is present on the annealed Au surface — indeed Figure 4.2 seems to support this as the plateaus are often surrounded by deep variances in height. Other studies [104–106] have shown via STM and AFM that this same phenomena occurs for Au(111). Contrast this to the case of the template-stripped surface where the terraces are smaller but the steps are of a single atomic height [40, 103] as is seen in Figure 4.3(a).

These differences in roughness (plateau size and step heights) help explain the results seen later in the FT-IR and contact angle characterization of the SAMs formed on the different Au surfaces as the substrate the monolayer forms on will influence its final configuration as evidenced by different metals (and

thus differing substrate crystallization), yielding different (internal) monolayer configurations [2, 27–29, 39, 40].

4.2 Spectroscopic Ellipsometry Data

4.2.1 Octadecanethiol SAMs on Evaporated, Annealed and Template-stripped Au

Spectroscopic ellipsometric measurements were performed on the octadecanethiol monolayer formed on the evaporated, annealed and template-stripped Au. The measured thickness of octadecanethiol adsorbed on each type of substrate is shown in Table 4.1.

Table 4.1: Spectroscopic ellipsometric thickness measurements of octadecanethiol adsorbed on evaporated, annealed, and template-stripped Au.

SAM Substrate	Octadecanethiol thickness (nm)
evaporated Au	2.0 ± 0.1^a
annealed Au	2.1 ± 0.1^a
template-stripped Au	2.0 ± 0.1^a

^a 95% confidence limit.

These thicknesses are in good agreement with those reported in the literature (see Fig.2.3), suggesting that the template-stripped octadecanethiol monolayer is consistent with earlier results for octadecanethiol monolayers on Au(111) [1, 2, 11, 33–35, 55] and that the monolayer has an *average* tilt from surface normal of around $\sim 30^\circ$. The difference in substrate roughness will have an effect on the ellipsometric measurements as the $n(\lambda)$ and $k(\lambda)$ curves for a crystalline alkanethiol SAM with CH_3 terminal group were generated from a monolayer

formed on evaporated Au. This change in roughness is estimated to contribute < 10% error to the annealed and template-stripped monolayers [33] which works out to ± 0.2 nm in this case. This was verified using the curve-fitting approach to Eq.(3.1) and inserting a 1 nm ‘rough’ layer on the substrate for a 2.2 nm model of an octadecanethiol SAM; the ‘new’ thickness was calculated to be 2.3 nm — a change of $\sim 5\%$.

4.2.2 Dodecanethiol SAMs on Template-stripped Au

Similarly the template-stripped dodecanethiol monolayer was measured via spectroscopic ellipsometer and a thickness of 1.6 ± 0.2 nm was obtained which also is similar to literature results for dodecanethiol monolayers on Au [3] (see Fig.2.3) and again suggests an *average* tilt of $\sim 30^\circ$ for the monolayer. A point of interest is that the optical constant curve — $n(\lambda)$, $k(\lambda)$ — is not the same as for octadecanethiol suggesting a different monolayer density/packing for the dodecanethiol monolayer although it is also possible that the difference in the number of CH₂ chains between the monolayers is solely responsible for the change in $n(\lambda)$ and $k(\lambda)$.

4.3 FT-IR data

In this thesis, the focus is on the C-H stretching region of the spectra; hence only the 2750–3050cm⁻¹ wavenumber region is shown.

4.3.1 Octadecanethiol Monolayers on Evaporated, Annealed and Template-stripped Au

Figure 4.4 shows the FT-IR spectra for octadecanethiol monolayers formed on evaporated, annealed, and template-stripped Au. It is clear from this figure

that the monolayer structures are similar to previous results for monolayers formed on Au; furthermore, the peak positions on all surfaces are consistent with literature results for an octadecanethiol SAM formed on non-template-stripped Au [1, 35] (see Table 2.1). Since it is well known that shifts in peak position are suggestive of changes in the ‘order/disorder’ of the monolayer [1, 34], these results suggest that the overall crystallinity of the monolayers formed on different Au substrates (evaporated, annealed, template-stripped) are similar — despite having been formed on surfaces of different roughness. That these peaks are ordered is borne out in comparing the liquid peaks of octadecanethiol to those of the monolayer formed on the template-stripped sample (in Fig.4.5). Since the liquid sample allows complete rotational freedom for the molecules compared to a crystalline monolayer, the clear shifts in the CH_2 peak positions and intensities represent an increase in the monolayer ‘order’ (i.e., the CH_2 peaks are oriented in the same direction and respond to the IR signal in the same way). The ‘disappearance’ of the $\nu_s(\text{CH}_3)$ signal in Fig.4.5 is likely due to the fact that the $\nu_s(\text{CH}_3)$ signal is weak enough that it is not possible to distinguish this peak reliably from the spectra noise. In addition, the template-stripped monolayer peaks are all narrow banded, suggesting a highly ordered structure [35, 57].

Based on these results and the measured monolayer thickness, it is expected that the $\sim 30^\circ$ *average* monolayer tilt reported in literature for an octadecanethiol monolayer on Au [1, 2, 57] will not change for either evaporated, annealed, or template-stripped surface.

To estimate the *average* tilt of the monolayer from the FT-IR spectra, a

simple model (shown in Fig.4.6) may be used along with a modified version of Debe's [14] RATIO method [40]. This is a first order approximation; nevertheless it provides a fair idea of the monolayer tilt. The original Debe model used the following relations:

$$r(yx) = \frac{\cos^2(\theta) + \alpha}{\sin^2(\Psi) \sin^2(\theta) + \alpha} \quad (4.1)$$

$$r(zx) = \frac{\sin^2(\theta) \cos^2(\Psi) + \alpha}{\sin^2(\Psi) \sin^2(\theta) + \alpha} \quad (4.2)$$

where θ , Ψ , and α are the angles shown in Fig.2.2 and r is the measured FT-IR peak intensities. The modified Debe method uses the ratio of the intensity of the two symmetric peaks, $\left(\frac{\nu_s(\text{CH}_2)}{\nu_s(\text{CH}_3)}\right)$, in both a KBr matrix and the monolayer on Au, and sets $\Psi = 0$ in Eq.(4.1) to obtain

$$r = \frac{\cos^2(\theta \pm 35^\circ)}{\cos^2(90^\circ - \theta)} = \frac{\frac{\nu_s(\text{CH}_2)}{\nu_s(\text{CH}_3)}_{\text{KBr}}}{\frac{\nu_s(\text{CH}_2)}{\nu_s(\text{CH}_3)}_{\text{SAM}}} \quad (4.3)$$

since $\nu_s(\text{CH}_3)$ is tilted at 34.75° from the surface normal when $\theta = 0^\circ$

Using Eq.(4.3), an *average* tilt angle of $\sim +31^\circ$ is obtained for the template-stripped monolayer (compared to calculated *average* tilts of $+27^\circ$ and $+28^\circ$ for the evaporated and annealed Au, respectively). This is a simplified single chain model which, although not exactly representative of the monolayer configuration on the surface, is nonetheless an approximate indicator of the average tilt of the monolayer. That the angles vary slightly between evaporated, annealed and template-stripped Au is not surprising as very little change in angle will generate fairly large changes in the model calculations (as shown in Fig.4.7).

4.3.2 Dodecanethiol Monolayers on Template-stripped Au

The dodecanethiol monolayer is compared in Figure 4.8 to the octadecanethiol monolayer formed on template-stripped Au. All the peak positions match except for the ν_a (CH_2) peak which shifts to 2920 cm^{-1} . Since the peak for the liquid state is 2924 cm^{-1} (see Fig. 4.5 and Table 2.1), this suggests that the monolayer is still quite crystalline but more disordered than the crystalline 2918 cm^{-1} octadecanethiol monolayer [1, 2]. The asymmetric CH_2 peak is also wider which is indicative of a greater degree of internal disorder in the monolayer. The ‘shoulder’ evident at 2938 cm^{-1} is due to the Fermi resonance peak which also contributes to the peak widening. Overall the monolayer still exhibits a crystalline structure relative to its liquid state (as is evident in Fig.4.5) but it is not as ordered as the octadecanethiol monolayer. Again using the modified Debe RATIO method, an average tilt of $+32^\circ$ is calculated for the dodecanethiol monolayer.

4.4 Contact Angle Data

4.4.1 Octadecanethiol on Evaporated, Annealed and Template-stripped Au

Figures 4.9 and 4.10 shows typical advancing contact angles for water on octadecanethiol SAMs on evaporated and annealed Au. The large difference between these advancing contact angles are statistically different if one looks at all the values measured for each probe liquid. The average of all the advancing contact angles for all the probe liquids used, together with the 95% confidence limit are shown in Table 4.2.

Figure 4.11 shows a typical advancing low-rate dynamic contact angle result obtained for water on an octadecanethiol SAM formed on template-stripped Au. Averaging the advancing contact angle results for water on the octadecanethiol template-stripped samples yields a mean value of $108.9^\circ \pm 1.1^\circ$ (95% confidence limit), which is close to that of the annealed Au ($106.9^\circ \pm 0.5^\circ$) and significantly lower than that of the evaporated Au ($119.1^\circ \pm 0.8^\circ$). The contact angle obtained for water on the octadecanethiol SAM formed on evaporated Au compares reasonably well with literature results (see Fig.2.4), especially if the $\pm 2^\circ$ goniometer [12] accuracy is considered. However, the annealed Au and template-stripped Au advancing contact angles are much lower than those reported in literature for alkanethiol CH_3 terminated SAMs. The results for all the advancing contact angles and liquids on octadecanethiol are presented in Table 4.2. From this table, it is obvious that the template-stripped and annealed samples exhibit essentially the same advancing contact angles for each of the liquids.

Table 4.2: A comparison of advancing contact angles (deg.) on octadecanethiol monolayers formed on: template-stripped Au (TS), annealed Au (A) and evaporated Au (E). Errors shown are the 95% confidence limits.

	TS (deg.)	A (deg.)	E (deg.)
water	108.9 ± 1.1	106.9 ± 0.5	119.1 ± 0.8
formamide	92.5 ± 1.7	92.4 ± 1.5	88.7 ± 0.8
ethylene glycol	84.1 ± 1.7	81.6 ± 2.4	81.5 ± 0.6
bromonaphthalene	^a	76.1 ± 0.9	67.2 ± 0.8
decanol	^a	53.2 ± 0.9	50.7 ± 0.5
hexadecane	44.1 ± 3.8	45.7 ± 0.8	45.4 ± 0.4

^a liquids not used to probe template-stripped samples

Similarly, a typical result for the receding low-rate dynamic contact angle for octadecanethiol monolayers on template-stripped Au is shown in Fig.4.12. Using this average receding contact angle, the hysteresis (H) can then be calculated for each sample using Eq.(2.2), where θ_a is the advancing contact angle and θ_r is the receding contact angle. The hysteresis for the SAMs on evaporated, annealed and template-stripped Au substrates are tabulated in Table 4.3. It is clear that the monolayer formed on the template-stripped Au surface exhibits considerably less hysteresis than either of the other two samples. This is somewhat surprising in the case of annealed Au versus template-stripped Au monolayers as their advancing contact angles are very similar. These results will be returned to momentarily; for the moment, recall that studies have attributed contact angle hysteresis to surface roughness [58–64], chemical inhomogeneity of the surface [65–72], molecular mobility and packing [73–75], liquid penetration and surface swelling [64, 76, 77], and liquid retention [64]. Based on these results, it is expected that the template-stripped sample has the ‘best’ surface quality since it has the lowest hysteresis for all liquids used.

Table 4.3: Experimental contact angle hysteresis (H) on SAMs of octadecanethiol adsorbed onto template-stripped Au (TS), annealed Au (A), and evaporated Au (E). Errors shown are the 95% confidence limits.

	TS	A	E
	H (deg.)	H (deg.)	H (deg.)
water	5.1 ± 4.7	14.6	18.9
formamide	8.4 ± 3.9	23.2	25.7
ethylene glycol	5.0 ± 3.1	11.8	23.1
hexadecane	3.2 ± 1.8	10.3	$< 25.4^a$

^a since $\theta_r < 20.0$ it is not possible to know exactly what the contact angle hysteresis is.

4.4.2 Dodecanethiol on Template-stripped Au

Similar to the results for octadecanethiol given above, template-stripped dodecanethiol advancing contact angles are very close to those of the octadecanethiol surface at $109.2^\circ \pm 1.9^\circ$; the complete results are summarized in Table 4.4. These results are interesting as other studies [2, 5, 10, 33, 39] have reported an increase in SAM hydrophobicity with chain length implying a contact angle for dodecanethiol less than that for octadecanethiol. That this is not reproduced here with the dodecanethiol monolayer formed on the template-stripped surface is clear from Table 4.4 where there is essentially no difference between the results for octadecanethiol and dodecanethiol formed on template-stripped Au substrates suggesting the same interfacial surface. This observation will be returned to later.

Table 4.4: A comparison of advancing contact angles for octadecanethiol (C18-TS) and dodecanethiol (C12-TS) monolayers formed on template-stripped Au. For reference θ_a on evaporated monolayers is shown for both octadecanethiol (C18-E) and dodecanethiol (C12-E). Errors shown are the 95% confidence limits.

	C12-TS θ_a (deg.)	C18-TS θ_a (deg.)	C12-E θ_a (deg.)	C18-E θ_a (deg.)
water	109.2 ± 1.9	108.9 ± 1.1	112^a	119.1 ± 0.8
formamide	94.0 ± 2.0	92.5 ± 1.7	b	88.7 ± 0.8

^a The advancing contact angle for water on evaporated dodecanethiol reported in ref.[5] was 112° . Note that the experimental surfaces used in [5] imply an evaporated Au surface similar to the one used here as the octadecanethiol advancing contact angle on the same surface is given as 117° (\sim the advancing contact angle obtained on the evaporated Au/octadecanethiol surfaces used here).

^b No data in [5] for formamide.

To complete the picture, the hysteresis calculated for the template-stripped

dodecanethiol monolayer in Table 4.5 is shown and compared to that for the template-stripped octadecanethiol monolayers and to that for evaporated Au surfaces for each monolayer. Again the same trend holds where the hysteresis is much less than that calculated for the evaporated monolayers.

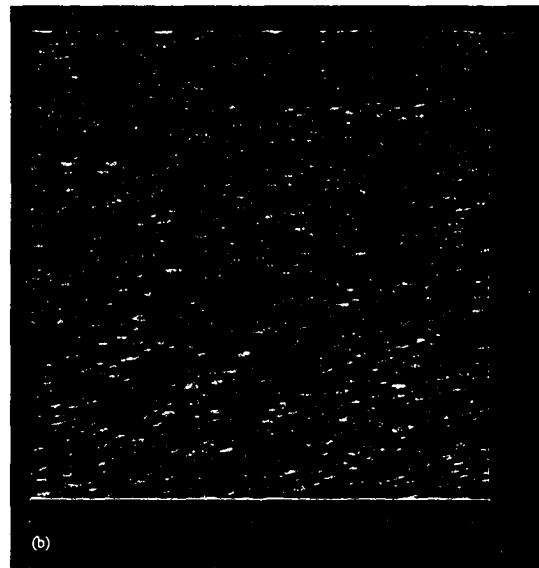
Table 4.5: A comparison of advancing contact angles and contact angle hysteresis of octadecanethiol (C18-TS) and dodecanethiol (C12-TS) monolayers formed on template-stripped Au. For reference hysteresis on evaporated monolayers is shown for both octadecanethiol (C18-E) and dodecanethiol (C12-E). Errors shown are the 95% confidence limits.

	C12-TS H (deg.)	C18-TS H (deg.)	C12-E H (deg.)	C18-E H (deg.)
water	4.7 ± 4.6	5.1 ± 4.7	24^a	25.7
formamide	13.0 ± 3.6	8.4 ± 3.9	b	18.9

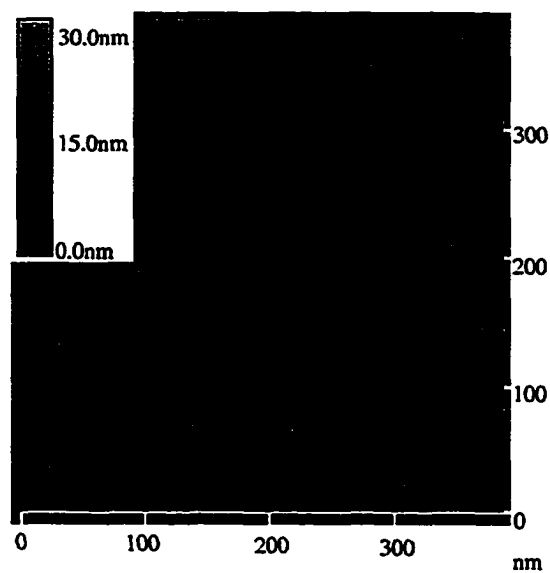
^a Hysteresis calculated from data in ref.[5] via Eq.(2.2).

^c No data in [5] for formamide.

These results suggest that ordered crystalline monolayers — i.e. $n \geq 12$ — will exhibit the same advancing contact angle despite chain length, providing that they are formed on ultra-flat surfaces. These results are not extended to monolayers where $n < 12$ since it is well known that alkanethiolate monolayers on Au where $n < 12$ are less ordered than those with more methylene chains [1, 2, 39]. Thus, to determine if the transition point changes on ultra-flat substrates more experiments are needed.



(a) 1 μm scan size (height scale 0 – 30nm)



(b) 0.3875 μm scan size (height scale 0 – 30nm)

Figure 4.1: 1 μm AFM scan size and a zoomed in 0.3875 μm scan size of evaporated Au (~ 100 nm) Ti adhesion layer (~ 10 nm) on Si substrate.

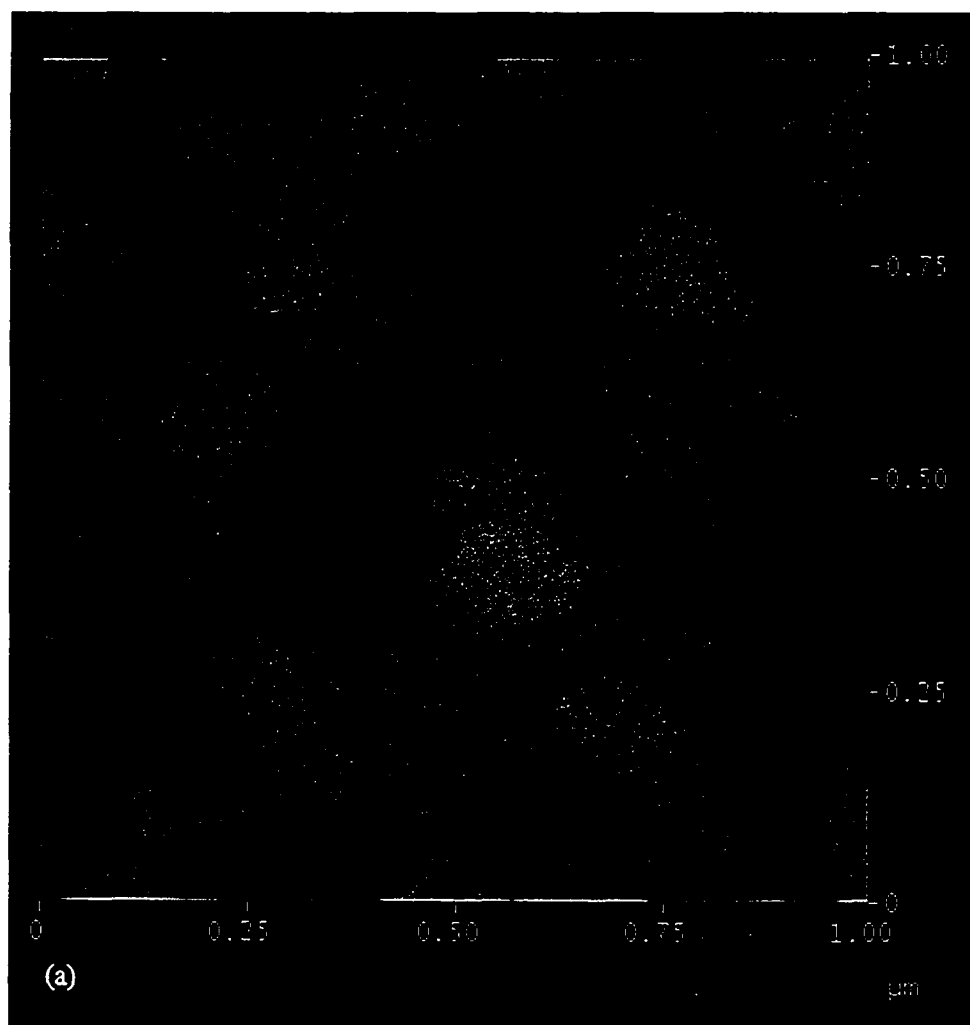
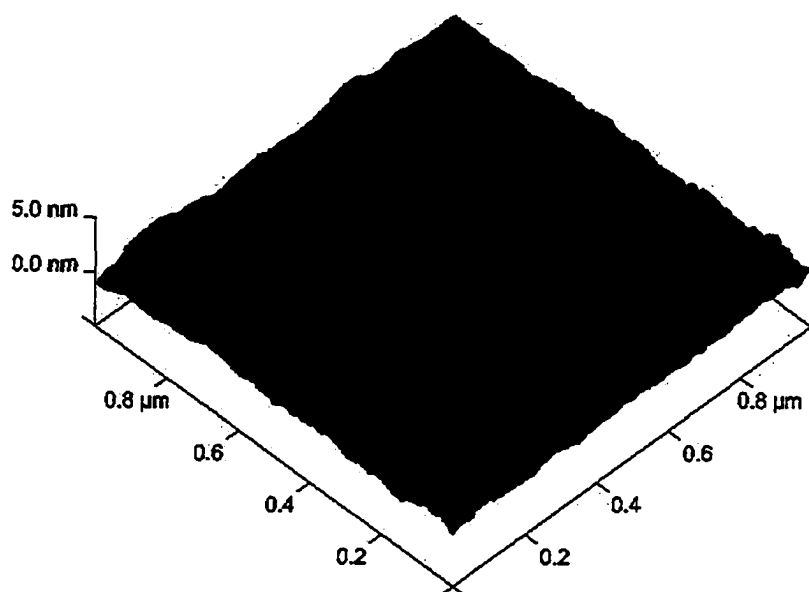
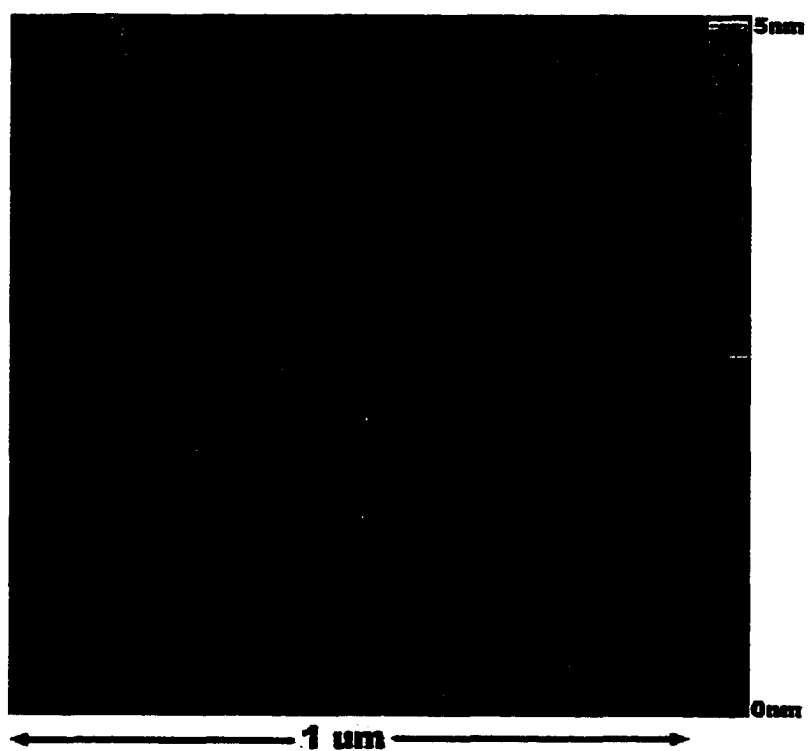


Figure 4.2: 1 μm AFM scan size of annealed Au (~ 100 nm) on Ti adhesion layer (~ 10 nm) on Si substrate.



(a) angle view



(b) top view

Figure 4.3: 1 μm scan size AFM images of template-stripped Au (angle and top view)

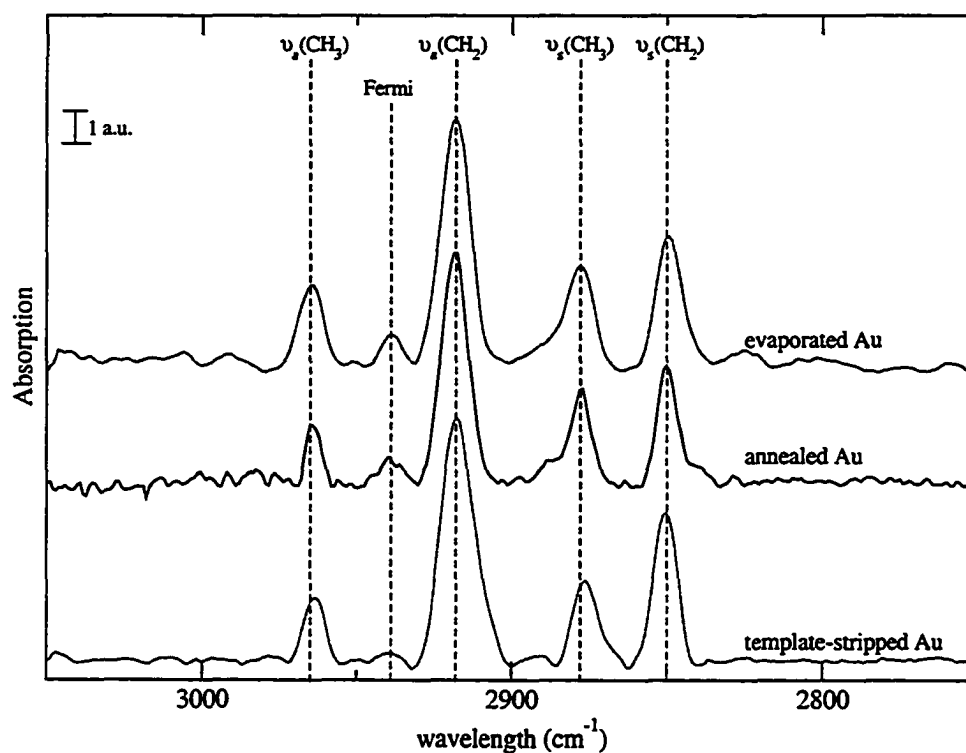


Figure 4.4: FT-IR spectra of octadecanethiol monolayers formed on template-stripped, annealed and evaporated Au. Peak positions: $\nu_a(\text{CH}_2)$ 2918 cm^{-1} , $\nu_s(\text{CH}_2)$ 2850 cm^{-1} , $\nu_a(\text{CH}_3)$ 2878 cm^{-1} (2877 cm^{-1} for the template-stripped sample) and $\nu_a(\text{CH}_3)$ 2965 cm^{-1} (2963 cm^{-1} for the template-stripped sample). The Fermi peak (ν_s , CH₃) is at 2938 cm^{-1} for the evaporated sample and 2940 cm^{-1} for the annealed and template-stripped samples. The spectra have been baseline corrected and offset for clarity.

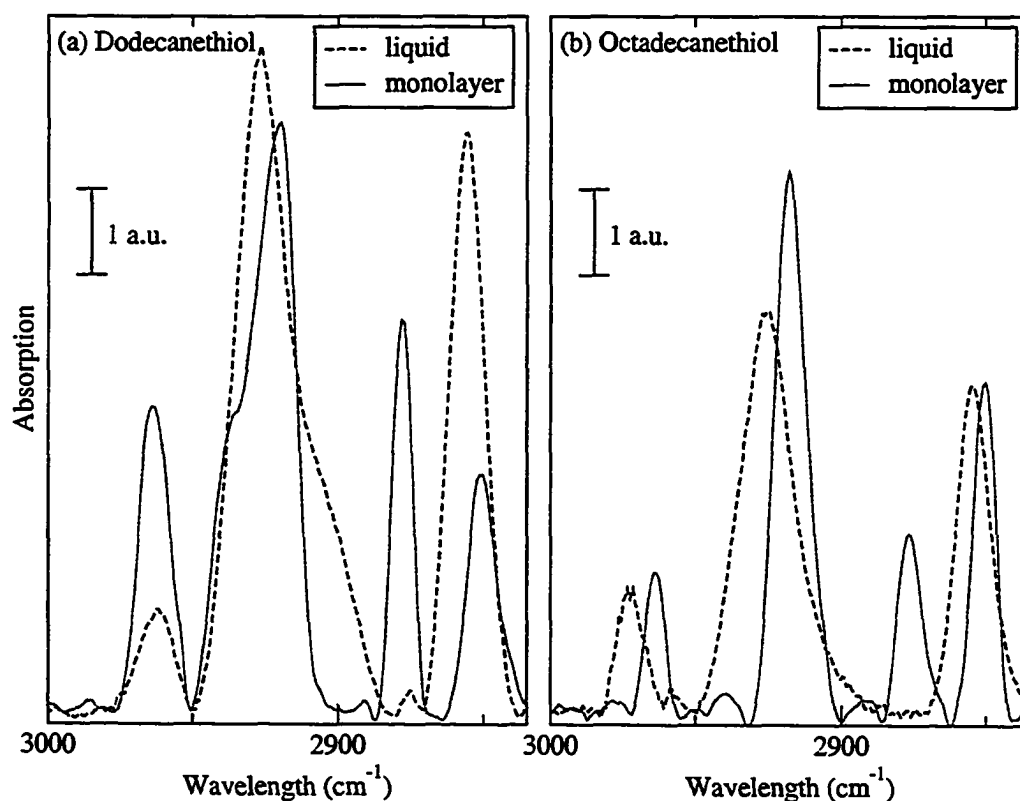


Figure 4.5: A comparison of liquid and crystalline monolayer spectra for: (a) $\text{CH}_3(\text{CH}_2)_{11}\text{SH}$, and (b) $\text{CH}_3(\text{CH}_2)_{17}\text{SH}$. The spectra have been baseline corrected and scaled to allow comparison.

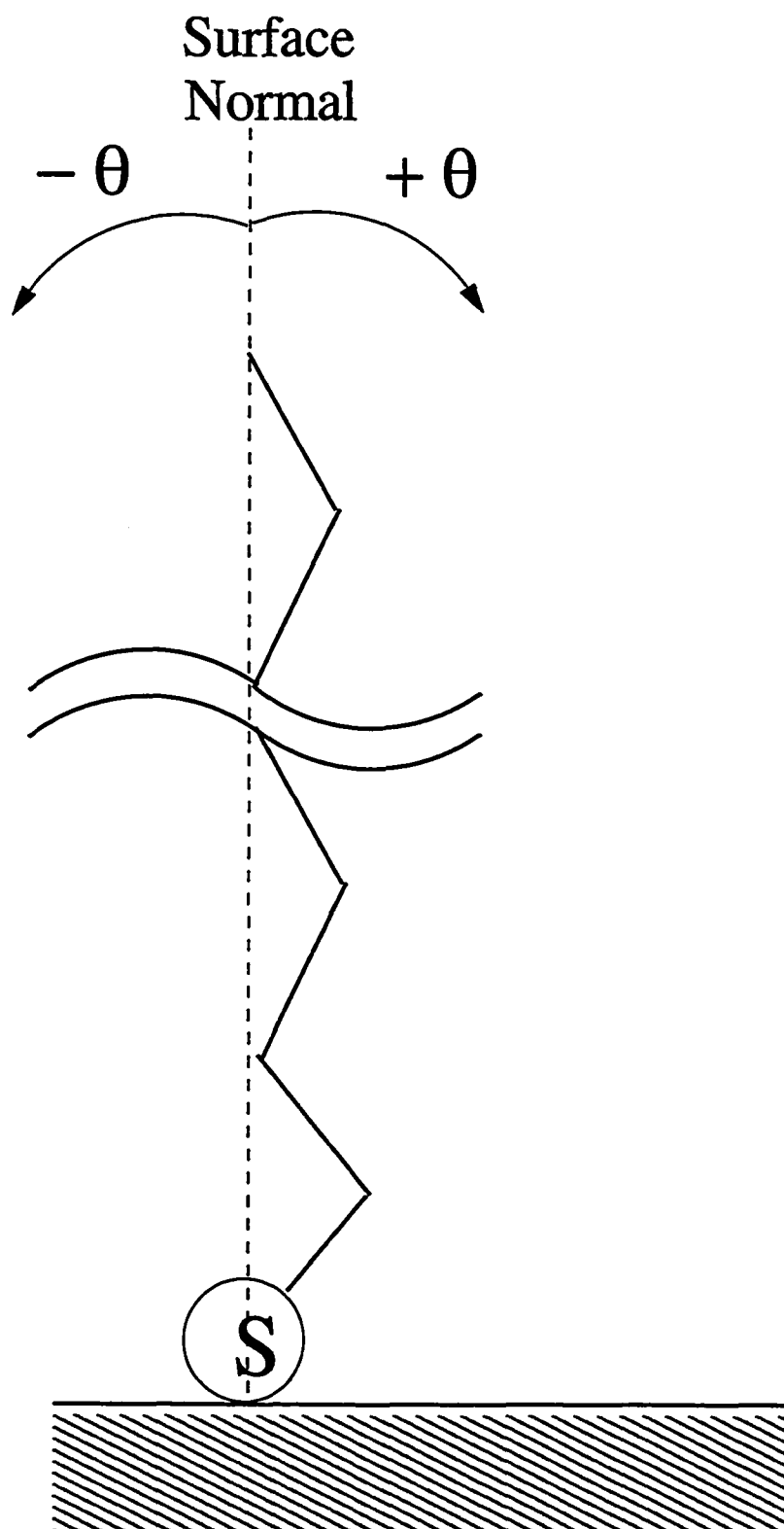


Figure 4.6: A simplified model used to estimate the *average* tilt of the alkylthiol monolayer using a modified version of Debe's [14] RATIO method.

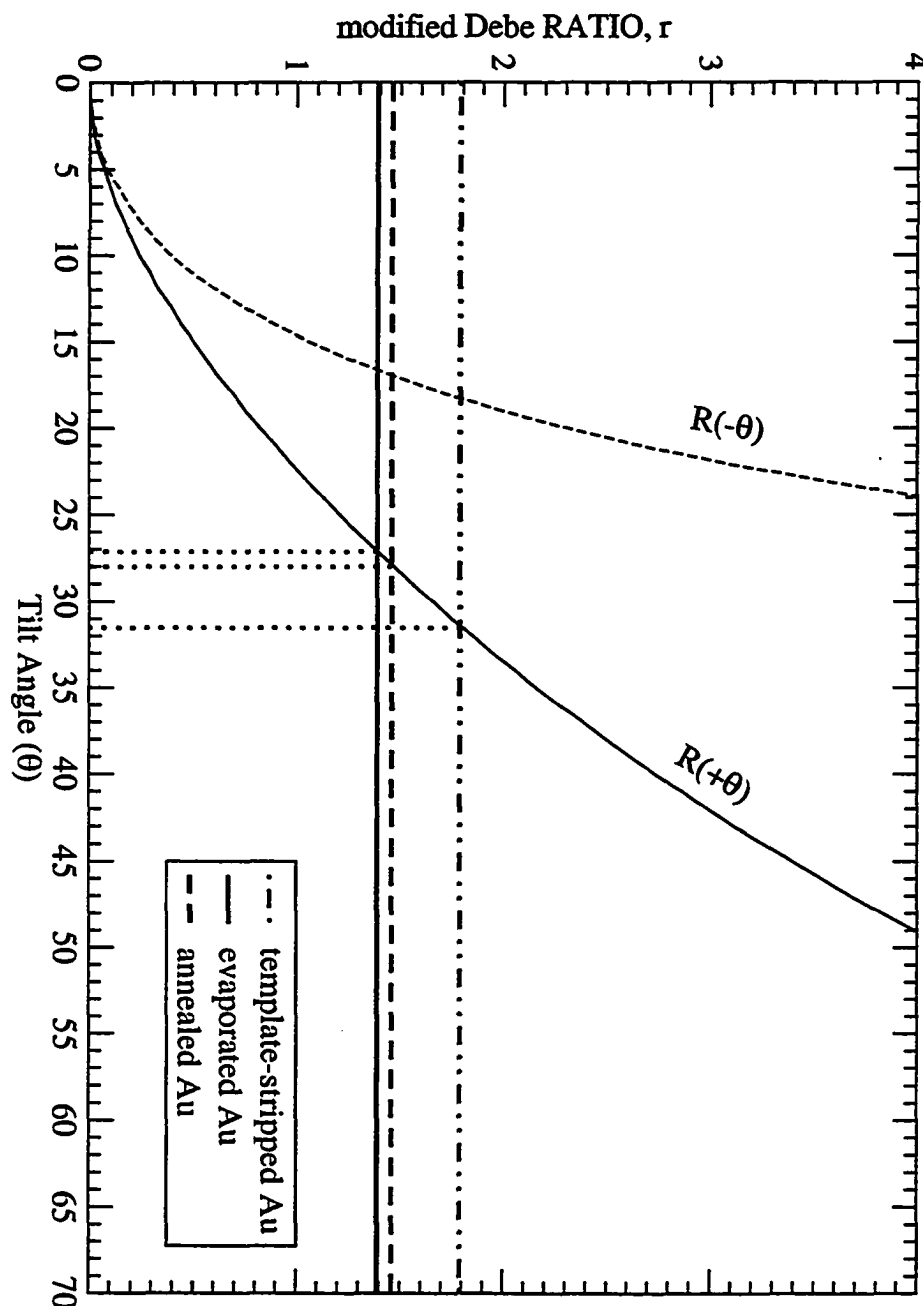


Figure 4.7: Result for modified Debe RATIO method for monolayers adsorbed on evaporated, annealed and template-stripped Au.

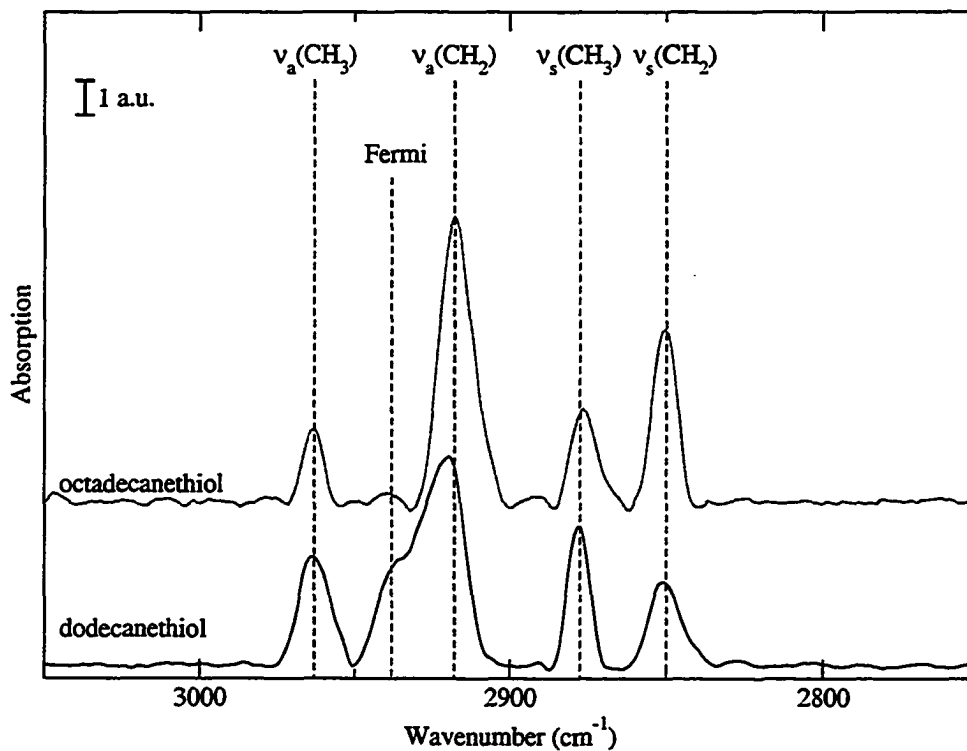


Figure 4.8: FT-IR spectra of octadecanethiol and dodecanethiol monolayers formed on template-stripped Au. The spectra have been baseline corrected and offset for clarity.

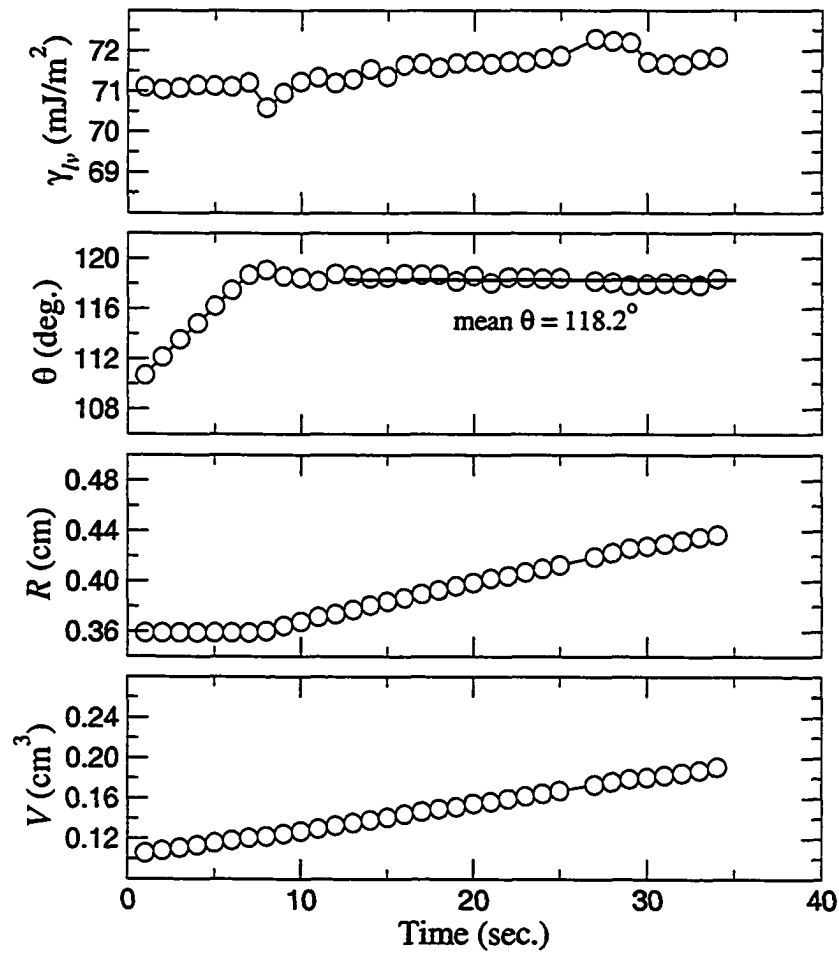


Figure 4.9: Typical advancing low-rate dynamic contact angle, θ_a , results for water on octadecanethiol monolayers formed on evaporated Au. As indicated in Fig.4.11 the mean values are taken once γ_{lv} and θ are constant.

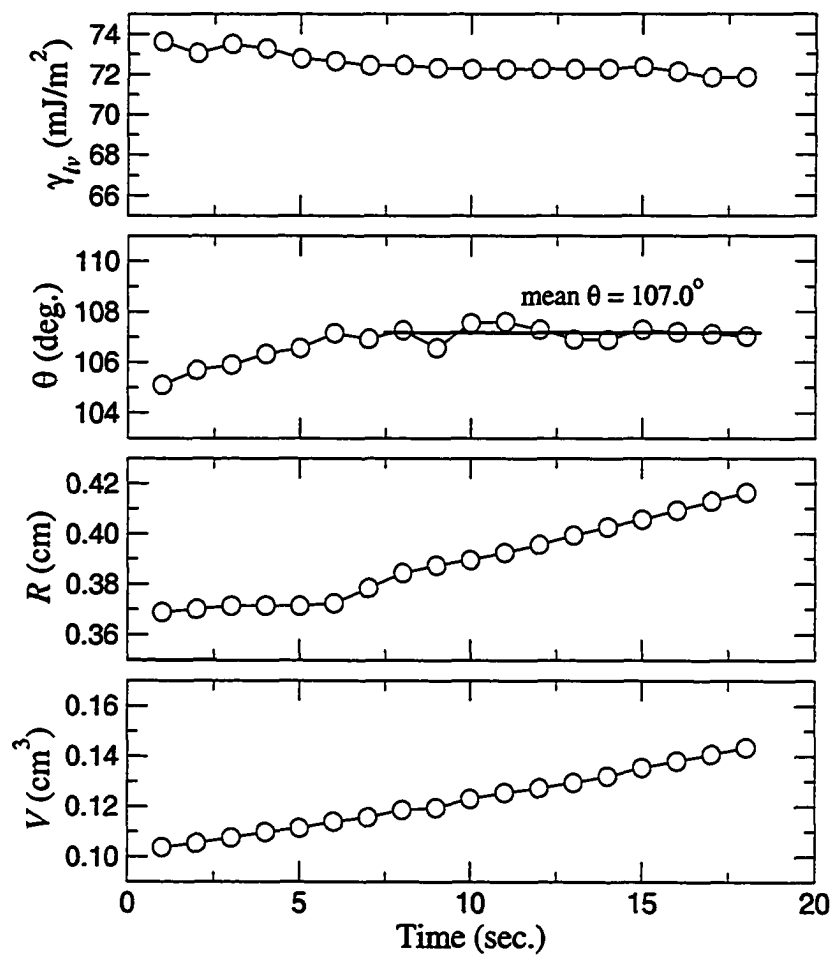


Figure 4.10: Typical advancing low-rate dynamic contact angle, θ_a , results for water on octadecanethiol monolayers formed on annealed Au. As indicated in Fig.4.11 the mean values are taken once γ_{lv} and θ are constant.

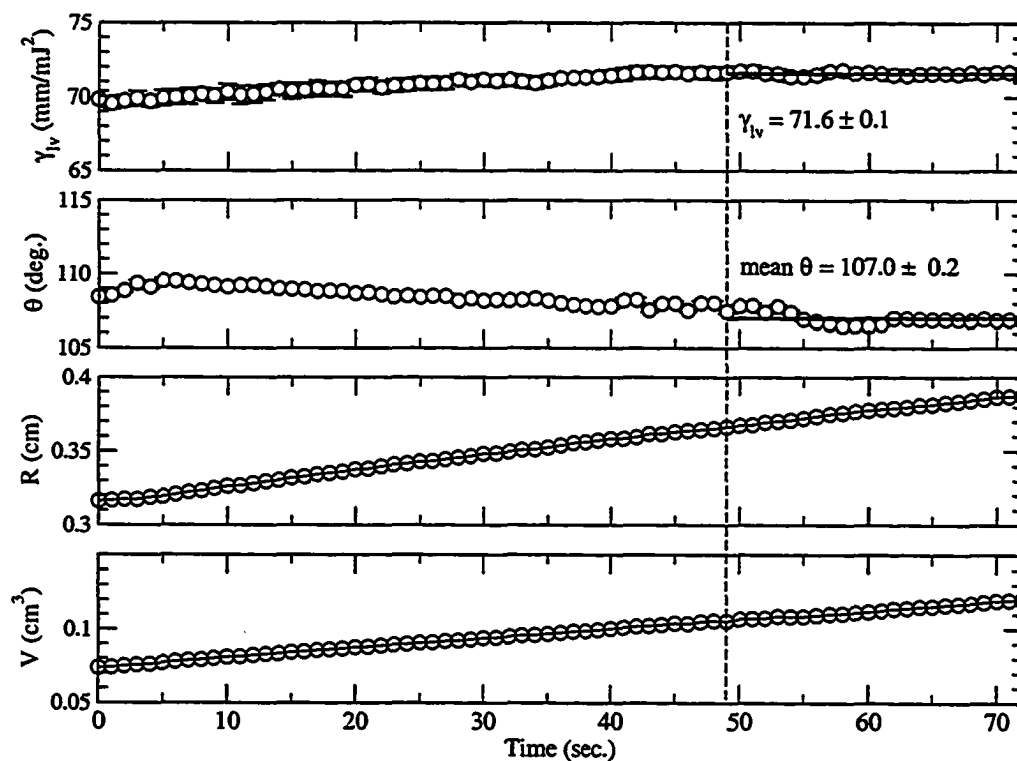


Figure 4.11: Typical low-rate dynamic advancing contact angle θ_a results for water on Octadecanethiol monolayers formed on template-stripped Au. As indicated the mean values are taken once γ_{lv} and θ are constant. It is clear that, as per the conditions set out earlier, at this point θ is constant as the drop volume (V) increases and the contact line radius (R) increases steadily.

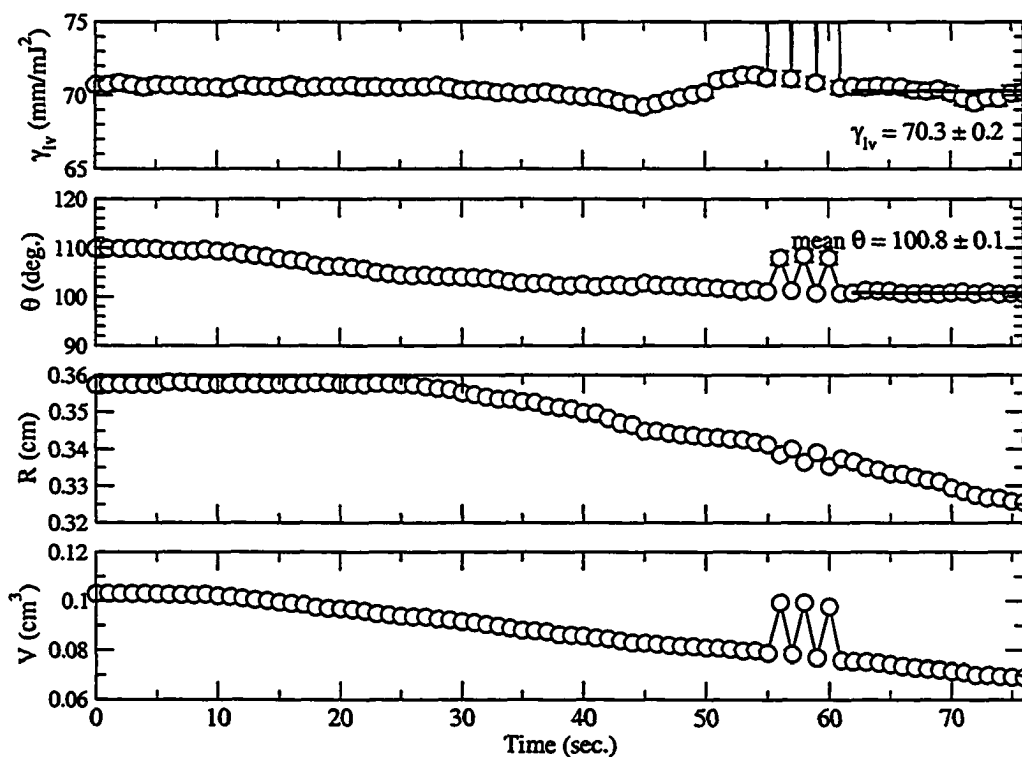


Figure 4.12: Typical low-rate dynamic receding contact angle θ_r results for water on Octadecanethiol monolayers formed on template-stripped Au. As indicated in Fig.4.11 the mean values are taken once γ_{lv} and θ are constant. It is clear that, as per the conditions set out earlier, at this point θ is constant as the drop volume (V) increases and the contact line radius (R) increases steadily. Note that, in this case, clear 'slip-stick' behavior (x-axis: 55–61) is demonstrated which must not be included when the contact angle is calculated — as noted earlier.

CHAPTER 5

DISCUSSION

Care must be taken in contact angle interpretation in order not to violate any commonly accepted assumptions. Nevertheless, it is possible to make several conclusions about the data presented here. Returning to the advancing contact angle data collected, the difference between the octadecanethiol SAMs adsorbed on evaporated and the annealed (and template-stripped) Au is first examined. These differing advancing contact angles are surprising given that the octadecanethiol SAM is formed on the same substrate (Au) and the solid-liquid system is presumably the same — an octadecanethiol monolayer at an *average* 30° tilt interacting with water (i.e., an expected CH₃ surface interacting with water). Looking only at the advancing water contact angle for octadecanethiol SAMs on evaporated Au, one might be tempted to conclude that a CH₃ surface shares the same solid surface tension as that of fluorocarbons FC721 and FC722 (water advancing contact angle of 118–120° [6, 107]) and one that is **higher** than that of Teflon poly(tetrafluoroethylene) (water advancing contact angle of 108–110° [95, 108]). This conclusion is questionable from a surface energetic point of view. Considering a CH₃ terminated polymer (hexatriacontane), whose surface quality was exceptional [13], the advancing contact angle reported was 105–107°. This

is much closer to the advancing contact angles for the octadecanethiol SAMs formed on annealed and template-stripped Au implying that these two surfaces are composed primarily of CH₃ molecules. To independently check the expected advancing contact angles for a CH₃ surface a study of polymer films by Grundke et. al [109] can be employed. They found that as the number of CH₂ groups increase in the side chains of the maleimide copolymers studied that the very polar maleimide groups were 'shielded' as well as the polar backbone groups, suggesting that eventually only the CH₃ would interact with the liquid if the *n*-alkyl side chains were long enough. Considering only the longer chain lengths (allowing considerable flexibility for chain rearrangement to lower the surface energy) and plotting the results of [109] in terms of the reciprocal of the number of CH₂ in the *n*-alkyl side chains as shown in Fig.5.1, an advancing contact angle of 108–109° for water is obtained for an infinite number of CH₂ groups (i.e., $1/x = 0$). This infinite CH₂ chain length would result in a hypothetically densely packed CH₃ surface since the side chains are long enough to allow arrangement in the lowest possible surface free energy. These values compare well with that for hexatriacontane (i.e., 105–107° for water [11, 13]). The advancing contact angle on annealed and template-stripped Au therefore is comparable to these values, suggesting a CH₃ surface exposed to the liquid. Since the annealed and template-stripped surfaces seem to be primarily a densely-packed CH₃ surface the question becomes: is this the case for the evaporated Au? From the FT-IR and spectroscopic ellipsometry data it is known that the structure is quite close to that of the other two surfaces so the monolayer formed on the evaporated Au is still expected to be primarily a CH₃ surface. For this case:

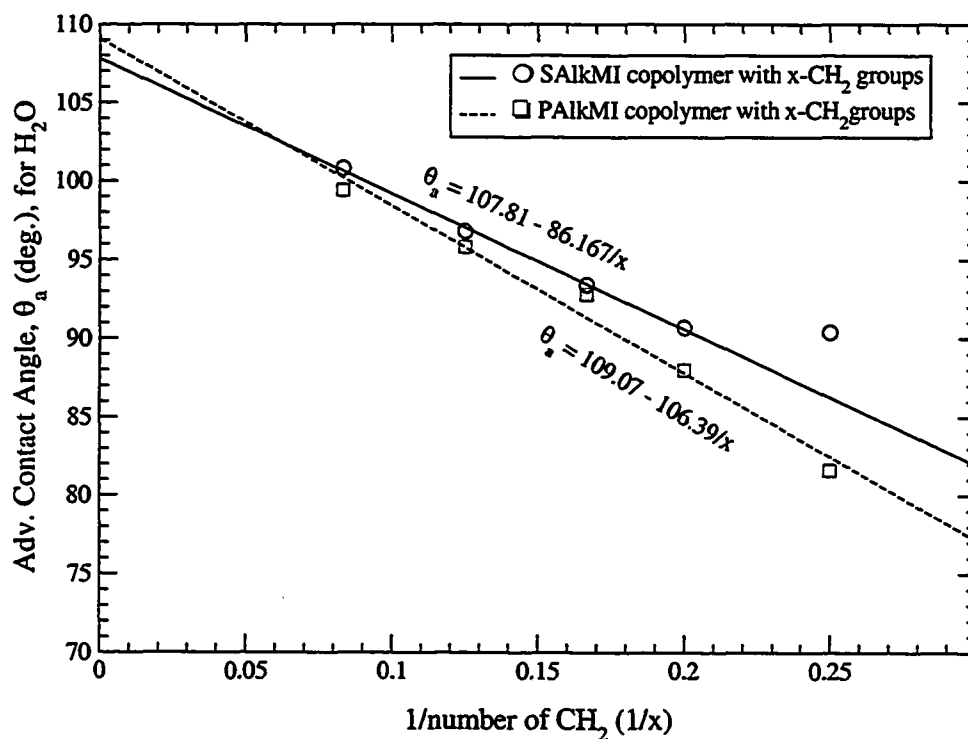


Figure 5.1: Advancing contact angles (θ_a) for two maleimide copolymers: [1] poly(propene-*alt*-N-(*n*-alkyl)maleimides) or (PAlkMI) [2] poly(styrene-*alt*-N-(*n*-alkyl)maleimides), (SAlkMI) versus the reciprocal of the number of CH_2 in the side chain, x

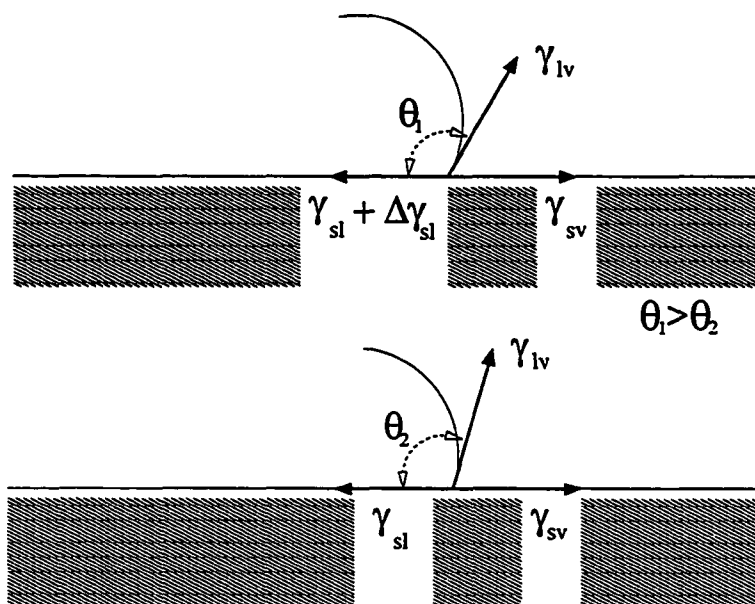


Figure 5.2: A schematic illustrating how the change in the surface structure changes the solid-liquid interfacial tension, γ_{sl} . Given that γ_{sv} and γ_{lv} remain unchanged the contact angle must increase due to $\Delta\gamma_{sl}$.

1. $\gamma_{sv} \sim \text{constant}$ since the surface is the same (CH_3 terminated surface),
and
2. $\gamma_{lv} = \text{constant}$ since the probe liquid is the same for both surfaces.

According to equation 1.1, this means that the change in contact angle on the SAM adsorbed onto the evaporated Au must therefore be due to an increase in γ_{sl} as illustrated in Figure 5.2. $\Delta\gamma_{sl}$ can be estimated for the evaporated Au using Eq.(1.1) and taking the difference in advancing contact angles with either the annealed or template-stripped SAMs, i.e.

$$\Delta\gamma_{sl} = \gamma_{lv}(\cos \theta_2 - \cos \theta_1) \quad (5.1)$$

Choosing the advancing water contact angles for the template-stripped (θ_2) and evaporated (θ_1) Au substrates, $\Delta\gamma_{sl} = 72.7(\cos 108.9^\circ - \cos 119.1^\circ) = 11.8$ mJ/m². In other words the solid-liquid surface tension is ~ 12 mJ/m² higher for the octadecanethiol SAM adsorbed on the evaporated Au substrate. Note that this difference also exists for the dodecanethiol monolayer (although the difference in contact angles is lower — likely due to a different mechanism which will be explained shortly). Using Eq.(5.1) to calculate $\Delta\gamma_{sl}$, for the template-stripped dodecanethiol monolayer water contact angles, yields ~ 3.3 mJ/m². The only difference between the three Au systems is in the underlying Au substrate topology. Thus, this must somehow be the contributing factor to these differences.

From the AFM data it can be concluded that:

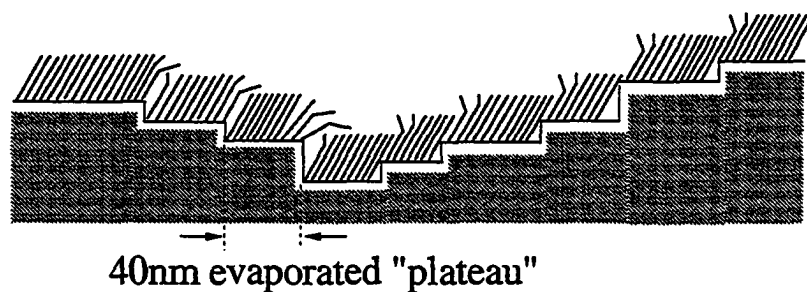
1. the evaporated monolayer has formed on a surface with plateaus ~ 40 – 50 nm in size and large multi-atomic steps between them,
2. the annealed monolayer has formed on a surface with large plateaus ~ 150 – 200 nm in size but also fairly large multi-atomic steps between them, and
3. the template-stripped monolayer has formed on a surface with terraces ~ 40 – 50 nm in size with atomic size steps (on average) between them.

From spectroscopic ellipsometry and FT-IR data it can be concluded that the monolayers on all three surfaces:

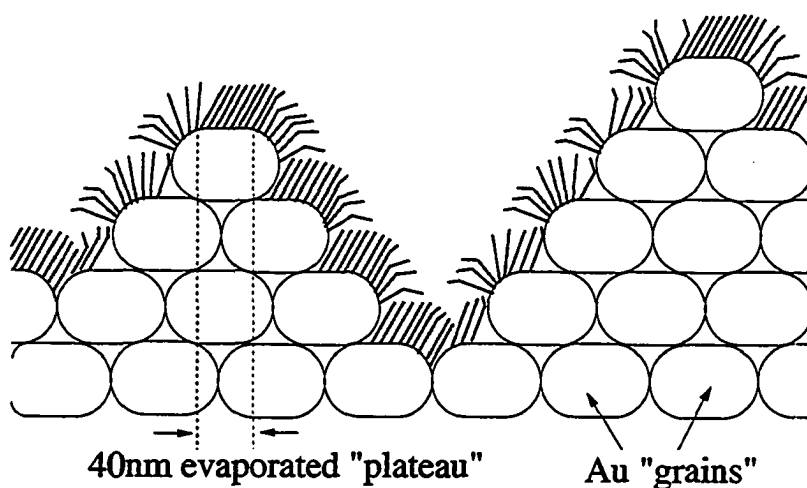
1. have the same *average* thicknesses

2. have similar *average* tilts of $\sim 30^\circ$, and
3. have similar crystalline structures.

Thus any model which seeks to explain these differences in contact angle must take into account these other pieces of experimental data. Figures 5.3 and 5.4 shows the monolayers modelled as formed on the different Au surfaces. The key difference is the terrace size and step heights which have already been elaborated upon. These features are incorporated into the substrates in Fig.5.3 and 5.4. These models make sense in that various STM studies [110–113] have imaged ‘line defects’ — missing alkanethiol molecule rows in the SAM or abrupt transitions to different SAM structure regimes — at the grain boundaries of Au(111) structures, i.e. the terrace and/or plateau edges. The effect of these differences in the surface topography of the monolayer are also shown: the monolayer on the evaporated and annealed Au has rotational freedom on the step edges, allowing the CH_2 backbone the ability to rotate as the neighboring molecules do not fully constrain the CH_2 chain (illustrated in Fig.5.3(a), 5.3(b) and 5.4(b)) while the template-stripped Au surface fully constrains the CH_2 backbone — even over the step edges (as illustrated in Fig.5.4(a)). That this constraint should not be chain-length dependent is obvious as shorter chains will still be constrained on the step edges on a template-stripped surface since the step heights are at atomic scale. Based on other studies where the onset of liquid-like disorder in alkanethiolates on Au were observed for $n \lesssim 8$ [1, 2, 39, 40], one can speculate that ‘disordered’ SAMs will occur in the same region on template-stripped Au surfaces as it has been shown that this cut-off point is different for different metals [40]. This point also helps explain the



(a) Evaporated — possibility A



(b) Evaporated — possibility B

Figure 5.3: A model illustrating the differences between monolayers ($n \geq 12$) formed on evaporated Au. The y-dimension is to scale, i.e. step height to molecule length, and molecules are tilted at 30° relative to surface normal. The x-direction is not to scale between the substrate and the SAM as it is not possible to fit the number of molecules required to accurately represent the SAM.

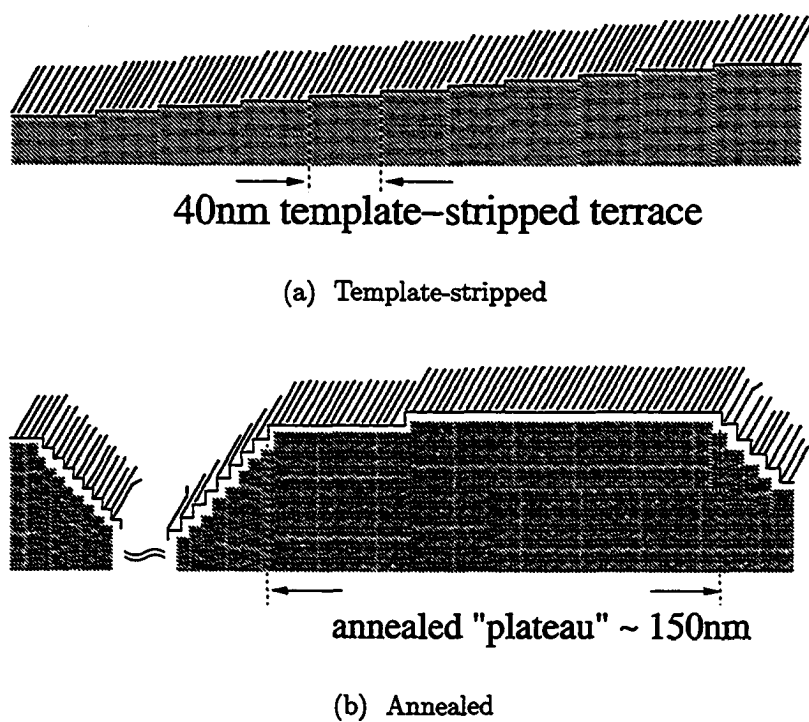


Figure 5.4: A model illustrating the differences between monolayers ($n \geq 12$) formed on template-stripped and annealed Au. The y-dimension is to scale, i.e. step height to molecule length, and molecules are tilted at 30° relative to surface normal. The x-direction is **not** to scale between the substrate and the SAM as it is not possible to fit the number of molecules required to accurately represent the SAM.

lower contact angles seen in literature for shorter CH₂ chain lengths as it is clear that once a certain chain length is reached, there is considerable ‘disorder’ exhibited (ie. rotational freedom) and the metal may be available to the liquid, further reducing the advancing contact angles. The mechanism of the higher contact angles seen on the evaporated Au monolayer is not clearly understood but it must be due to ‘defects’ at the CH₃ surface caused by the substrate roughness (and illustrated in Fig.5.3(a) and 5.3(b)). The fact that these ‘defects’ are not observable via FT-IR is not surprising as even with a 0.000016 m² IR area the amount of ‘defects’ relative to the surface will be very low. A quick estimation shows this to be the case. The IR area is known to be 1.6×10⁻⁵ m² and assuming an area per molecule of 21.4 Å² [27] suggests 7.5×10²³ molecules per IR area. If ‘defects’ are assumed around the perimeter of every plateau this means ~ 1.4–2.8×10¹⁷ molecules are defective (depending upon whether the number of terraces/IR area is for annealed or template-stripped Au). This suggests defects in the order of 0.00002–0.00004% — a clear over-estimation as all plateau perimeters are assumed defective over their **whole** length. This in turn seems to indicate that the increase in γ_{sl} for the evaporated Au adsorbed SAM is linked somehow to the difference in either surface topography or the molecular bonding between CH₃ molecules and/or the first few molecules in the CH₂ backbone. That the CH₃ bonding is different between the annealed and template-stripped surfaces is clear as both the ν_s and ν_a CH₃ peaks have shifted to a more crystalline position for the template-stripped sample as seen in Fig.4.4. This, however, does not seem to affect the advancing contact angles as they are very similar for these two surfaces. There do not appear to be many

differences between the internal structures of the CH₂ backbone, judging by the peak widths in Fig.4.4. Thus, it appears that the most likely cause of $\Delta\gamma_{sl}$ is the surface topography, i.e. roughness. This is interesting because although both the annealed and evaporated Au share the same PV roughness, the frequency of this roughness is higher on the evaporated sample if one compares average plateau size.

It is also possible based on the experimental results to assert that, at a minimum, fully crystalline SAMs (compared to evaporated Au and possibly even annealed Au) exist on template-stripped Au when $n \geq 12$. This explains the similar advancing contact angles and contact angle hysteresis between octadecanethiol and dodecanethiol monolayers formed on template-stripped Au — since the internal structure of the monolayer has little to no effect on the wettability of the interface [3, 4, 114] as the depth to which the liquid can sense is believed to be ~ 5 Å for water and ~ 2 Å for hexadecane [115, 116] and as a result the interfacial surface of both monolayers is expected to consist of an atomically flat, densely packed CH₃ surface. Therefore, since γ_{sv} , γ_{sl} , and γ_{lv} are thermodynamic properties of the surface and liquid, and each system is the ‘same’, θ_Y (ie. θ_a) should therefore be the same between these different chain-length monolayers. That this is essentially the case speaks to the remarkable similarity of the interfacial surface despite the different internal ordering of octadecanethiol and dodecanethiol monolayers (as inferred from the FT-IR results shown in Figs.4.5 and 4.8).

SAMs formed on evaporated Au show significant scatter from the hexatriacontane curve as is seen clearly in Fig.5.5, in good agreement with literature

results (see Fig.2.6). As pointed out earlier, this scatter is due to changes in the solid-liquid interfacial tensions which in turn changes the advancing contact angles. If the (same) monolayers formed on both the annealed and template-stripped Au substrates are examined, it is found that they fall roughly on the hexatriacontane curve as seen in Fig.5.6. The scatter has disappeared and the curves are quite smooth, thus confirming that the experimental results are compatible with Eqs. 2.3–2.5. These results are yet more evidence that the dodecanethiol and octadecanethiol share the same interfacial characteristics; if this were not the case, they would ‘scatter’ relative to each other as seen in the evaporated Au case in Fig.5.5.

The equation of state approach can also be used to calculate the solid-vapor interfacial tension [12]. The equation of state for solid-liquid surface tension can be written as:

$$\gamma_{sl} = \gamma_{lv} + \gamma_{sv} - 2\sqrt{\gamma_{lv}\gamma_{sv}}e^{-\beta(\gamma_{lv}-\gamma_{sv})^2} \quad (5.2)$$

Combining Eq.(5.2) with Eq.(1.1) yields

$$\cos \theta_Y = -1 + 2\sqrt{\frac{\gamma_{sv}}{\gamma_{lv}}}e^{-\beta(\gamma_{lv}-\gamma_{sv})^2} \quad (5.3)$$

Using the FORTRAN code given in [12] and $\beta = 0.0001247 \text{ (m}^2/\text{mJ)}^2$ [12, 16], γ_{sv} can be calculated using the different advancing contact angles. The results are summarized in Table 5.1. The expected γ_{sv} for a CH_3 -terminated surface is 19–20 mJ/m^2 [11] so these calculated γ_{sv} again add evidence that the surface is composed primarily of CH_3 molecules.

Interestingly enough, even though annealed and template-stripped Au adsorbed SAMs share the same advancing contact angle, thicknesses, average

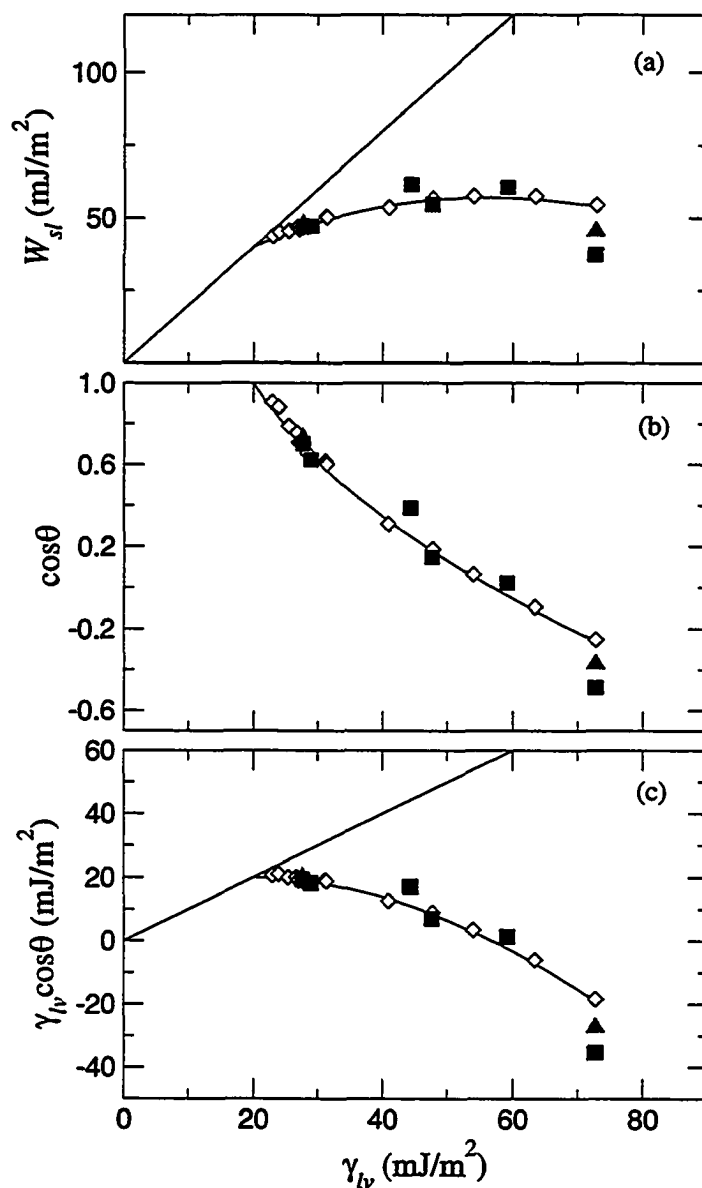


Figure 5.5: (a) The solid-liquid work of adhesion, W_{sl} , (b) the cosine of the contact angle, $\cos\theta$, and (c) the liquid-vapor surface tension times the cosine of the contact angle, $\gamma_{lv} \cos\theta$, versus the liquid vapor surface tension, γ_{lv} shown for hexatriacontane (\diamond) and SAMs of octadecanethiol (\blacksquare) and dodecanethiol (\blacktriangle) formed on evaporated Au. Data for dodecanethiol shown here is calculated from [5].

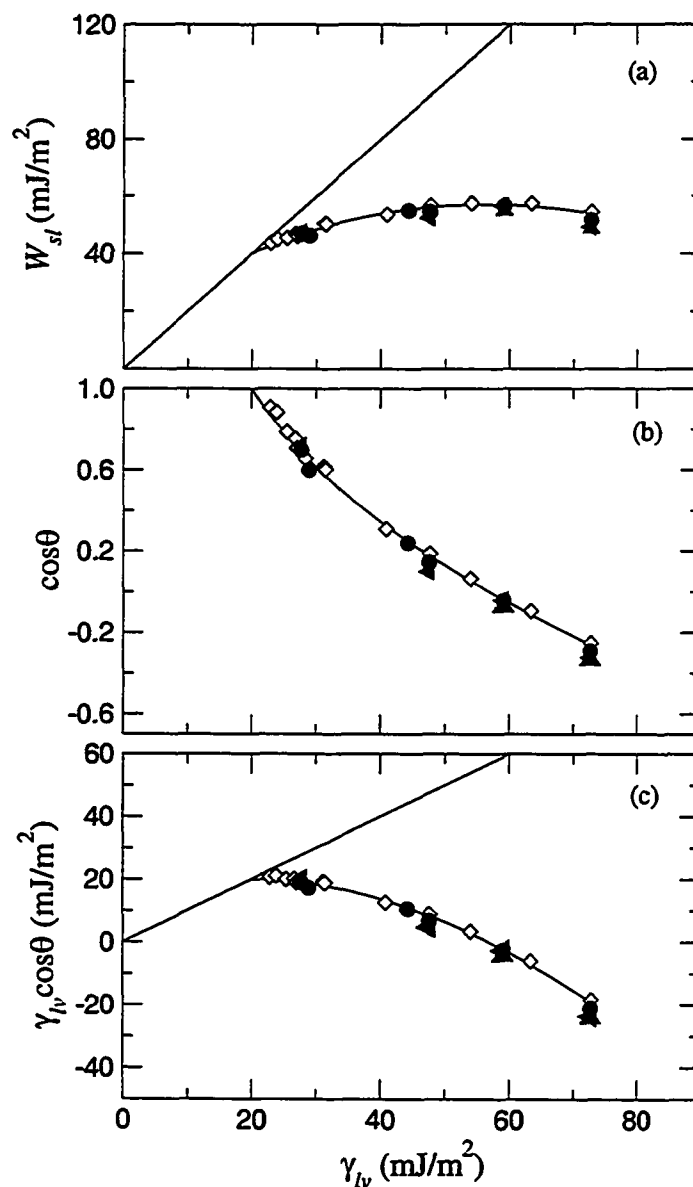


Figure 5.6: (a) The solid-liquid work of adhesion, W_{sl} , (b) the cosine of the contact angle, $\cos\theta$, and (c) the liquid-vapor surface tension times the cosine of the contact angle, $\gamma_{lv} \cos\theta$, versus the liquid vapor surface tension, γ_{lv} . Data shown for hexatriacontane (\diamond) and octadecanethiol formed on annealed Au (\bullet) are compared to SAMs of octadecanethiol (\blacktriangleleft) and dodecanethiol (\blacktriangle) formed on template-stripped Au.

Table 5.1: γ_{sv} calculated using the equation of state approach with $\beta = 0.0001247 \text{ (m}^2/\text{mJ)}^2$

	A			TS	
	γ_{lv} (mJ/m ²)	θ_a (deg.)	γ_{sv} (mJ/m ²)	θ_a (deg.)	γ_{sv} (mJ/m ²)
water	72.7	106.9	18.8	108.9	17.7
formamide	59.1	92.4	19.9	92.5	19.8
ethylene glycol	47.6	81.6	19.1	84.1	18.0
bromonaphthalene	44.3	76.1	19.8	^a	-
decanol	28.9	53.2	18.9	^a	-
hexadecane	27.6	45.7	20.2	44.1	20.6
average			19.5 ± 0.6^b		19.0 ± 1.9^b

^a no data collected for these probe liquids on template-stripped samples

^b 95% confidence limit

monolayer tilt and internal crystalline structure, there exists a noticeable difference in contact angle hysteresis between the two Au monolayers. This is not likely to be due to changes in the monolayer crystalline structure as it has been shown in other studies [2–4, 114] that wetting is not affected by differing internal structures of the same monolayer and in any case these monolayers appear to be similar to other Au systems in literature in terms of average tilt, FT-IR results and thicknesses. Thus, the only difference that must change the hysteresis between these systems is the terrace size and step height as these differences are expected to also show up on the monolayer interfacial surface. This being the case, it is expected that it is primarily the reduced step height for the template-stripped samples which is the main contributor to this reduced contact angle hysteresis as the liquid will not as likely to be ‘trapped’ (see Fig.5.3 and 5.4) by the shallow step heights of the template-stripped surface. Indeed, considering the mean van der Waal diameter of water of 2.82 Å [117], it can be

seen that this is very close to the step height on the template-stripped surface. Lam et. al [64] showed that a large 'bulky' molecule (OCMTS, ie. octamethyl-clotetrasiloxane, with a mean molecular dia. $\sim 9 \text{ \AA}$) had a very small hysteresis on the system they were studying. They hypothesize that liquid retention is the cause of contact angle hysteresis. If this is the case, the receding contact angle would decrease since retention of the liquid on the solid surface will increase the solid surface tension (since the liquids they chose as probe liquids — and the ones used here — have a liquid interfacial tension greater than the solid surface tension). Thus liquid retention would result in a higher hysteresis since θ_a would not change but θ_r would be smaller. Since the size of the OCMTS molecule compared to the step heights on the surface is relatively large this would make liquid retention difficult and thus the low contact angle hysteresis reported. In the template-stripped case, this is also the case due to the fact that the average step height is on the order of several angstroms; thus the step height and the liquid molecule are on the same order of magnitude, making liquid retention more difficult. Judging by the very low values of contact angle hysteresis tabulated in both Tables 4.3 and 4.4, the template-stripped adsorbed SAMs are close to an 'ideal' Young's surface.

CHAPTER 6

CONCLUSIONS AND FUTURE WORK

6.1 Conclusion

This thesis set out to answer the question of the anomaly in contact angle measurements between literature results for SAMs and for similarly terminated surfaces that were not monomolecular films. AFM data showed that the template-stripped Au surface consisted of 40–50 nm terraces separated by atomic step heights. Spectroscopic ellipsometry results yielded a monolayer thickness in line with previous literature results for -thiol/Au systems and indirectly pointed to a similar average monolayer tilt. FT-IR results showed a crystalline monolayer that does not differ significantly from those reported in the literature and a calculated average monolayer tilt agreed with both the spectroscopic ellipsometry results and those in literature. Low-rate dynamic contact angle experiments yield an advancing contact angle consistent with what is expected for a closely-packed smooth methyl surface. In addition, the contact angle hysteresis obtained on the template-stripped surface seems to indicate a largely defect free surface of high quality. Taken together, these results seem to indicate that it is possible to construct an ‘ideal’ Young’s surface with SAMs on a template-stripped Au surface. In addition it was shown that this surface is possible to

achieve on at least a dodecanethiol monolayer and that it may be achievable at even lower chain lengths on template-stripped Au substrates.

6.2 Future Work

The work done in this thesis can be extended to:

1. exploring the effect of different chain lengths of the alkanethiol, especially in the region $n < 12$,
2. using low-rate dynamic contact angles to characterize some of the other template systems used [88–94], particularly the mica based Au templates as they will produce larger terraces which will combine large terraces with atomic step heights,
3. different metal substrate/SAM systems which will vary the underlying SAM structure as in [40].
4. extending recent work done by Tavana et. al [118] and Lam et. al [64] using large ‘bulky’ molecules to eliminate liquid penetration and retention. Using these molecules on a template-stripped substrate adsorbed SAM may lead to zero hysteresis.
5. impacting drops as the template-stripped/SAM system allows access to an ultra-flat, chemically tailorable surface, which can be used in the exploration of the impact of topography roughness in the impacting droplet spreading and recoil.

BIBLIOGRAPHY

- [1] M. D. Porter, T. B. Bright, D. L. Allara, and C. E. D. Chidsey. Spontaneously Organized Molecular Assemblies. 4. Structural Characterization of *n*-Alkyl Thiol Monolayers on Gold by Optical Ellipsometry, Infrared Spectroscopy, and Electrochemistry. *J. Am. Chem. Soc.*, 109:3559, 1987.
- [2] P. E. Laibinis, G. M. Whitesides, D. L. Allara, Y. T. Tao, A. N. Parikh, and R. G. Nuzzo. Comparison of the Structures and Wetting Properties of Self-Assembled Monolayers of *n*-Alkanethiols on the Coinage Metal Surfaces, Cu, Ag, Au. *J. Am. Chem. Soc.*, 113:7152, 1991.
- [3] G. K. Jennings and P. E. Laibinis. Self-Assembled *n*-Alkanethiolate Monolayers on Underpotentially Deposited Adlayers of Silver and Copper on Gold. *J. Am. Chem. Soc.*, 119:5208, 1997.
- [4] P. E. Laibinis and G. M. Whitesides. ω -Terminated Alkanethiols on Surfaces of Copper, Silver, and Gold Have Similar Wettabilities. *J. Am. Chem. Soc.*, 114:1990, 1992.
- [5] J. A. M. Sondag-Huethorst and L. G. J. Fokkink. Electrical Double Layers on Thiol-modified Polycrystalline Gold Electrodes. *J. Electro. Chem.*, 367:49, 1994.

- [6] D. Y. Kwok, R. Lin, M. Mui, and A. W. Neumann. Low-rate dynamic and static contact angles and the determination of solid surface tensions. *Colloids Surf. A*, 116:63, 1996.
- [7] D. Y. Kwok, C. N. C. Lam, A. Li, A. Leung, R. Wu, E. Mok, and A. W. Neumann. Low-Rate Dynamic Contact Angles on Noninert Poly(propene-*alt* - *N*-(*n*-alkyl)maleimide) Copolymers by an Automated Axisymmetric Drop Shape Analysis (ADSA-P). *Langmuir*, 14:2221, 1998.
- [8] D. Y. Kwok, A. Leung, A. Li, C. N. C. Lam, R. Wu, E. Mok, and A. W. Neumann. Low-rate dynamic contact angles on poly(*n*-butyl methacrylate) and the determination of solid surface tensions. *Colloid Polym. Sci.*, 276:459, 1998.
- [9] E. B. Troughton, C. D. Bain, G. M. Whitesides, R. G. Nuzzo, D. L. Allara, and M. D. Porter. Monolayer Films Prepared by the Spontaneous Self-Assembly of Symmetrical and Unsymmetrical Dialkyl Sulfides from Solution onto Gold Substrates: Structure, Properties, and Reactivity of Constituent Functional Groups. *Langmuir*, 4:365, 1988.
- [10] C. D. Bain, E. B. Troughton, Y.-T. Tao, J. Evall, G. M. Whitesides, and R. G. Nuzzo. Formation of Monolayer Films by the Spontaneous Assembly of Organic Thiols from Solution onto Gold. *J. Am. Chem. Soc.*, 111:321-335, 1989.
- [11] J. Yang, K. Isaacson, J. Han, and D. Y. Kwok. Effects of Surface Defects, Polycrystallinity, and Nanostructure of Self-Assembled Monolayers

- for Octadecanethiol Adsorbed onto Au on Wetting and Its Surface Energetic Interpretation. *Langmuir*, 19(22):9213, 2003.
- [12] D. Y. Kwok and A. W. Neumann. Contact angle measurement and contact angle interpretation. *Adv. Colloid Interface Sci.*, 81:167, 1999.
- [13] A. W. Neumann. Contact Angles and their Temperature Dependence: Thermodynamic Status, Measurement, Interpretation and Application. *Adv. Colloid Interface Sci.*, 4(2-3):105, 1974.
- [14] M. K. Debe. Extracting physical structure information from thin organic films with reflection absorption infrared spectroscopy. *J. Appl. Phys.*, 55(9):3354, 1983.
- [15] T. Young. An Essay on the Cohesion of Fluids. *Philos. Trans. R. Soc. London*, 95:65, 1805.
- [16] D. Y. Kwok. Contact Angles: Measurements, Interpretation, Adhesion and Molecular Theory. *Recent Res. Devel. Physical Chem.*, 6:651, 2002.
- [17] W. A. Zisman. volume Contact Angle, Wettability and Adhesion of *Advances in Chemistry Series*. American Chemical Society, Washington, D.C., 1964.
- [18] F. M. Fowkes. Attractive Forces at Interfaces. *Ind. Eng. Chem.*, 56(12):40, 1964.
- [19] J. K. Spelt and D. Li. Applied Surface Thermodynamics. Marcel Dekker, New York, 1996.

- [20] R. J. Good and C. J. van Oss. *Modern Approaches to Wettability: Theory and Applications*. Plenum Press, New York, 1992.
- [21] O. Driedger, A. W. Neumann, and P. J. Sell. Über Die Grenzflächenenergetische Zustandsfunktion. *Kolloid Z.Z. Polym.*, 201(1):52, 1965.
- [22] A. W. Neumann, R. J. Good, C. J. Hope, and M. Sejpal. An Equation-of-state Approach to Determine Surface Tensions of Low Energy Solids from Contact Angles. *J. Colloid Interface Sci.*, 49(2):291, 1974.
- [23] D. K. Owens and R. C. Wendt. Estimation of the Surface Free Energy of Polymers. *J. Appl. Polym. Sci.*, 13(8):1741, 1969.
- [24] C.J. van Oss, M. K. Chaudhury, and R. J. Good. Interfacial Lifshitz-van der Waals and Polar Interactions in Macroscopic Systems. *J. Chem. Rev.*, 88:927, 1988.
- [25] D. Y. Kwok, T. Gietzelt, K. Grundke, , H. J. Jacobasch, and A. W. Neumann. Contact Angle Measurements and Contact Angle Interpretation. 1. Contact Angle Measurements by Axisymmetric Drop Shape Analysis and a Goniometer Sessile Drop Technique. *Langmuir*, 13(10):2880, 1997.
- [26] D. Y. Kwok, C. N. C. Lam, A. Li, A. Leung, R. Wu, E. Mok, and A. W. Neumann. Measuring and Interpreting Contact Angles: A Complex Issue. *Colloids Surf., A*, 142:219, 1998.
- [27] A. Ulman. Formation and Structure of Self-Assembled Monolayers. *Chem. Rev.*, 96:1533, 1996.

- [28] R. K. Smith, P. A. Lewis, and P. S. Weiss. Patterning self-assembled monolayers. *Prog. Surf. Sci.*, 75:1, 2004.
- [29] F. Schreiber. Structure and Growth of Self-Assembling Monolayers. *Progress in Surf. Sci.*, 65:151, 2000.
- [30] W. C. Bigelow, D. L. Pickett, and W. A. Zisman. Oleophobic Monolayers. 1. Films Absorbed from Solution in Non-Polar Liquids. *J. Colloid Sci.*, 1(6):513, 1946.
- [31] R. L. Shuler and W. A. Zisman. Wave-Damping and Film-pressure Studies of Polymethylsiloxane Monolayers on Organic Liquid Substrates. *J. Phys. Chem.*, 79(14):139, 1975.
- [32] M. K. Bennett and W. A. Zisman. Surface Chemical Properties of Highly Fluorinated Polymers. *Adv. Chem. Ser.*, 8:199, 1975.
- [33] D. L. Allara and R. G. Nuzzo. Spontaneously Organized Molecular Assemblies. 1. Formation, Dynamics, and Physical Properties of *n*-Alkanoic Acids Adsorbed from Solution on an Oxidized Aluminum Surface. *Langmuir*, 1:45, 1985.
- [34] D. L. Allara and R. G. Nuzzo. Spontaneously Organized Molecular Assemblies. 2. Quantitative Infrared Spectroscopic Determination of Equilibrium Structures of Solution-Adsorbed *n*-Alkanoic Acids on an Oxidized Aluminum Surface. *Langmuir*, 1:52, 1985.
- [35] R. G. Nuzzo, F. A. Fusco, and D. L. Allara. Spontaneously Organized Molecular Assemblies 3. Preparation and Properties of Solution Adsorbed

- Monolayers of Organic Disulfides on Gold Surfaces. *J. Am. Chem. Soc.*, 109:2358, 1987.
- [36] G. Hähner, C. H. Wöll, M. Buck, and M. Grunze. Investigation of Intermediate Steps in the Self-Assembly of *n*-Alkanethiols on Gold Surfaces by Soft X-Ray Spectroscopy. *Langmuir*, 9:1955, 1993.
- [37] O. Dannenberger, M. Buck, and M. Grunze. Self-Assembly of *n*-Alkanethiols: A Kinetic Study by Second Harmonic Generation. *J. Phys. Chem. B*, 103:2202, 1999.
- [38] M. Himmelhaus, F. Eisert, M. Buck, and M. Grunze. Self-Assembly of *n*-Alkanethiol Monolayers. A Study by IR-Visible Sum Frequency Spectroscopy (SFG). *J. Phys. Chem. B*, 104:576, 2000.
- [39] J. C. Love, D. B. Wolfe, R. Haasch, M. L. Chabinyc, K. E. Paul, G. M. Whitesides, and R. G. Nuzzo. Formation and Structure of Self-Assembled Monolayers of Alkanethiolates on Palladium. *J. Am. Chem. Soc.*, 125:2597, 2003.
- [40] J. J. Blackstock, Z. Li, D. R. Stewart, K. Isaacson, D. Y. Kwok, M.R. Freeman, and J.-B. D. Green. in preparation 2004.
- [41] S. E. Creager, L. A. Hockett, and G. K. Rowe. Consequences of Microscopic Surface Roughness for Molecular Self-Assembly. *Langmuir*, 8:854, 1992.
- [42] H. S. Kim, S. J. Lee, N. H. Kim, J. K. Yoon, H. K. Park, and K. Kim. Ad-

- sorption Characteristics of 1,4-Phenylene Diisocyanide on Gold Nanoparticles: Infrared and Raman Spectroscopy Study. *Langmuir*, 19:6701, 2003.
- [43] G. Chen, P. Hui, K. Pita, P. Hing, and L. Kong. Conductivity drop and crystallites redistribution in gold film. *Appl. Phys. A - Mat. Sci. Proc.*, DOI: 10.1007/s00339-003-2321-3, 2003.
- [44] B. H. Flowers Jr., T. L. Wade, J. W. Garvey, M. Lay, U. Happek, and J. L. Stickney. Atomic layer epitaxy of CdTe using automated electrochemical thin-layer flow deposition reactor. *J. Electro. Chem.*, 524-525:273, 2003.
- [45] J. J. Blackstock, Z. Li, M. R. Freeman, and D. R. Stewart. Ultra-flat Platinum Surfaces from Template-Stripping of Sputter Deposited Films. *Surface Science*, 546:87, 2003.
- [46] S. W. Han, C. H. Kim, S. H. Hong, Y. K. Chung, and K. Kim. Azobenzene-Incorporated Alkanethiol Monolayer Film on Au(111): Reflection-Absorption Infrared Spectroscopy and Atomic Force Microscopy Study. *Langmuir*, 15:1579-1583, 1999.
- [47] M. Fang, D. M. Kaschak, A. C. Sutorik, and T. E. Mallouk. A "Mix and Match" Ionic-Covalent Strategy for Self-Assembly of Inorganic Multilayer Films. *J. Am. Chem. Soc.*, 119:12184, 1997.
- [48] M. A. Ansell, E. B. Cogan, and C. J. Page. Coordinate Covalent Cobalt-Diisocyanide Multilayer Thin Films Grown One Molecular Layer at a Time. *Langmuir*, 16:1172, 2000.

- [49] R. R. Shah and N. L. Abbott. Orientational Transitions of Liquid Crystals Driven by Binding of Organoamines to Carboxylic Acids Presented at Surfaces with Nanometer-Scale Topography. *Langmuir*, 19:275–284, 2003.
- [50] A. C. Zeppenfeld, S. L. Fiddler, W. K. Ham, B. J. Klopfenstein, and C. J. Page. Variation of Layer Spacing in Self-Assembled Hafnium-1, 10-Dacnediylbis(phosphonate) Multilayers As Determined by Ellipsometry and Grazing Angle X-ray Diffraction. *J. Am. Chem. Soc.*, 116:9158–9165, 1994.
- [51] M. L. Schilling, H. E. Katz, S. M. Stein, S. F. Shane, W. L. Wilson, S. Buratto, S. B. Ungashe, G. N. Taylor, T. M. Putvinski, and C. E. D. Chidsey. Structural Studies of Zirconium-Alkylphosphonate Monolayers and Multilayer Assemblies. *Langmuir*, 9:2156, 1993.
- [52] D. Laurent and J. B. Schmidt. Multilayer Assemblies of Redox Polyelectrolytes. *Langmuir*, 13:1552, 1997.
- [53] E. S. Forzani, M. A. Pérez, M. L. Teijelo, and E. J. Calvo. Redox Driven Swelling of Layer-by-layer Enzyme – Polyelectrolyte Multilayers. *Langmuir*, 18:9867, 2002.
- [54] E. S. Forzani, M. Otero, M. A. Pérez, M. L. Teijelo, and E. J. Calvo. The Structure of Layer-by-Layer Self-Assembled Glucose Oxidase and Os(Bpy)₂CIPyCH₂NH –Poly(allyamine) Multilayers: Ellipsometric and Quartz Crystal Microbalance Studies. *Langmuir*, 18:4020, 2002.
- [55] P. E. Laibinis, R. G. Nuzzo, and G. M. Whitesides. Structure of Mono-

- layers Formed by Coadsorption of Two *n*-Alkanethiols of Different Chain Lengths on Gold and its Relation to Wetting. *J. Phys. Chem.*, 96:5097, 1992.
- [56] S. D. Evans, E. Urankar, A. Ulman, and N. Ferris. Self-Assembled Monolayers of Alkanethiols Containing a Polar Aromatic Group: Effects of the Dipole Position on Molecular Packing, Orientation, and Surface Wetting Properties. *J. Am. Chem. Soc.*, 113:4121, 1991.
- [57] R. G. Nuzzo, L. H. Dubois, and D. L. Allara. Fundamental Studies of Microscopic Wetting on Organic Surfaces. 1. Formation and Structural Characterization of a Self-Consistent Series of Polyfunctional Organic Monolayers. *J. Am. Chem. Soc.*, 112:558, 1990.
- [58] F. E. Bartell and J. W. Shepard. Surface Roughness as Related to Hysteresis of Contact Angles 1. The System Paraffin-Water-Air. *J. Phys. Chem.*, 57:211, 1953.
- [59] R. E. Johnson Jr. and R. H. Dettre. *Adv. Chem. Ser.*, 43:112, 1964.
- [60] J. D. Dick, R. J. Good, and A. W. Neumann. Thermodynamics of Contact Angles II. Rough Solid Surfaces. *J. Colloid Interface Sci.*, 53(2):235, 1975.
- [61] J. F. Oliver, C. Huh, and S. G. Mason. Apparent Contact Angle of Liquids on Finely-grooved Solid Surfaces - SEM Study. *J. Adhes.*, 8:223, 1977.
- [62] J. F. Oliver, C. Huh, and S. G. Mason. Experimental Study of Some Effects of Solid-Surface Roughness on Wetting. *Colloids Surf.*, 1:79, 1980.

- [63] J. F. Oliver and S. G. Mason. Liquid Spreading on Rough Metal Surfaces. *J. Mater. Sci.*, 15:431, 1980.
- [64] C. N. C. Lam, N. Kim, D. Hui, D. Y. Kwok, M. L. Hair, and A. W. Neumann. The Effect of Liquid Properties to Contact Angle Hysteresis. *Colloids and Surfaces A*, 189:265, 2001.
- [65] F. J. Good. A Thermodynamic Derivation of Wenzel's Modification of Young's Equation for Contact Angles; Together with a Theory of Hysteresis. *J. Am. Chem. Soc.*, 74:5041, 1952.
- [66] R. E. Johnson Jr. and R. H. Dettre. Contact Angle Hysteresis. III. Study of an Idealized Heterogeneous Surface. *J. Phys. Chem.*, 68:1744, 1964.
- [67] R. H. Dettre and R. E. Johnson Jr. Contact Angle Hysteresis. IV. Contact Angle Measurements on Heterogeneous Surfaces. *J. Phys. Chem*, 69:1507, 1965.
- [68] A. W. Neumann and R. J. Good. Thermodynamics of Contact Angles. I. Heterogeneous Solid Surfaces. *J. Colloid Interface Sci.*, 38:341, 1972.
- [69] L. W. Schwartz and S. Garoff. Contact Angle Hysteresis on Heterogeneous Surfaces. *Langmuir*, 1:219, 1985.
- [70] A. Marmur. Contact Angle Hysteresis on Heterogeneous Smooth Surfaces. *J. Colloid Interface Sci.*, 168:40, 1994.
- [71] E. L. Decker and S. Garoff. Using Vibrational Noise to Probe Energy Barriers Producing Contact Angle Hysteresis. *Langmuir*, 12:2100, 1996.

- [72] E. L. Decker and S. Garoff. Contact Line Structure and Dynamics on Surfaces with Contact Angle Hysteresis. *Langmuir*, 13:6321, 1997.
- [73] W. Chan and T. J. McCarthy. Layer-by-Layer Deposition: A Tool for Polymer Surface Modification. *Macromolecules*, 30:78, 1997.
- [74] A. Y. Fadeev and T. J. McCarthy. Trialkylsilane Monolayers Covalently Attached to Silicon Surfaces: Wettability Studies Indicating that Molecular Topography Contributes to Contact Angle Hysteresis. *Langmuir*, 15:3759, 1999.
- [75] J. P. Youngblood and T. J. McCarthy. Ultrahydrophobic Polymer Surfaces Prepared by Simultaneous Ablation of Polypropylene and Sputtering of Poly(tetrafluoroethylene) Using Radio Frequency Plasma. *Macromolecules*, 32:6800, 1999.
- [76] R. V. Sedev, C. J. Budziak, J. G. Petrov, and A. W. Neumann. Dynamic Contact Angles at Low Velocities. *J. Colloid Interface Sci.*, 159:392, 1993.
- [77] R. V. Sedev, J. G. Petrov, and A. W. Neumann. Effect of Swelling of a Polymer Surface on Advancing and Receding Contact Angles. *J. Colloid Interface Sci.*, 180:36, 1996.
- [78] D. Y. Kwok, A. Leung, C. N. C. Lam, A. Li, R. Wu, and A. W. Neumann. Low-Rate Dynamic Contact Angles on Poly(methyl methacrylate) and the Determination of Solid Surface Tensions. *J. Colloid Interface Sci.*, 206:44, 1998.

- [79] D. Y. Kwok, C. N. C. Lam, A. Li, K. Zhu, R. Wu, and A. W. Neumann. Low-Rate Dynamic Contact Angles on Polystyrene and the Determination of Solid Surface Tensions. *Polym. Eng. Sci.*, 38:1675, 1998.
- [80] D. Y. Kwok, A. Li, C. N. C. Lam, R. Wu, S. Zschoche, K. Pöschel, T. Gietzelt, K. Grundke, H. J. Jacobasch, and A. W. Neumann. Low-rate dynamic contact angles on poly[styrene-*alt*-(hexyl/10-carboxydecyl(90/10)maleimide)] and the determination of solid surface tensions. *Macromol. Chem. Phys.*, 200(5):1121, 1999.
- [81] D. Y. Kwok, C. N. C. Lam, and A. W. Neumann. Wetting Behavior and Solid Surface Tensions for a 70:30 Copolymer of Polystyrene and Poly(methyl methacrylate). *Colloid J.*, 62(3):324, 2000.
- [82] D. Y. Kwok, R. Wu, A. Li, and A. W. Neumann. Contact angle measurements and interpretation: wetting behavior and solid surface tensions for poly(alkyl methacrylate) polymers. *J. Adhes. Sci. Technol.*, 14(5):719, 2000.
- [83] D. Y. Kwok, A. Li, and A. W. Neumann. Low-Rate Dynamic Contact Angles on Poly(methyl methacrylate/ethyl methacrylate, 30/70) and the Determination of Solid Surface Tensions. *J. Polym. Sci., Part B: Polym. Phys.*, 37:2039, 1999.
- [84] O. I. del Río, D. Y. Kwok, R. Wu, J. M. Alvarez, and A. W. Neumann. Contact Angle Measurement by Axisymmetric Drop Shape Analysis and an Automated Polynomial Fit Program. *Colloid Surf., A*, 143:197, 1998.

- [85] G. H. E. Hellwig and A. W. Neumann. page 687. 5th International Congress on Surface Activity, Section B, 1968.
- [86] G. H. E. Hellwig and A. W. Neumann. Temperature Dependence of Moistening of Cholesteryl Acetate by Water. *Kolloid Z. Z. Polym.*, 40:229, 1969.
- [87] D. Y. Kwok, C. N. C. Lam, A. Li, and A. W. Neumann. Low-rate Dynamic Contact Angles on Poly(methyl methacrylate/*n*-butyl methacrylate) and the Determination of Solid Surface Tensions. *J. Adhesion*, 68:229, 1998.
- [88] M. Hegner, P. Wagner, and G. Semenza. Ultralarge atomically flat template-stripped Au surfaces for scanning probe microscopy. *Surface Science*, 291:39, 1993.
- [89] P. Wagner, M. Hegner, H.-J. Güntherodt, and G. Semenza. Formation and in Situ Modification of Monolayers Chemisorbed on Ultraflat Template-Stripped Gold Surfaces. *Langmuir*, 11:3867, 1995.
- [90] R. F. Knarr and R. A. Quon. Direct Force Measurements at the Smooth Gold/Mica Interface. *Langmuir*, 14:6414, 1998.
- [91] P. Samorí, J. Diebel, H. Löwe, and J. P. Rabe. Template-Stripped Gold Supported on Ni as a Substrate for SAMs. *Langmuir*, 15:2592, 1999.
- [92] J. Diebel, H. Löwe, P. Samorí, and J. P. Rabe. Fabrication of large-scale ultra-smooth metal surfaces by a replica technique. *Appl. Phys. A*, 73:273, 2001.

- [93] C. I. Priest, K. Jacobs, and J. Ralston. Novel Approach to the Formation of Smooth Gold Surfaces. *Langmuir*, 18:2438, 2002.
- [94] P. Gupta, K. Loos, A. Korniaikov, C. Spagnoli, M. Cowman, and A. Ulman. Facile Route to Ultraflat SAM-Protected Gold Surfaces by “Amphiphile Splitting”. *Angew. Chem. Int. Ed.*, 43:520, 2004.
- [95] K. Grundke, T. Bogumil, T. Gietzelt, H. J. Jacobasch, D. Y. Kwok, and A. W. Neumann. Wetting Measurements on Smooth, Rough and Porous Solid Surfaces. *Prog. Colloid Polym. Sci.*, 101:58, 1996.
- [96] D. Y. Kwok, H. Ng, and A. W. Neumann. Experimental Study on Contact Angle Patterns: Liquid Surface Tension Less Than Solid Surface Tensions. *J. Colloid Interface Sci.*, 225(2):323, 2000.
- [97] R. G. Greenler. Infrared Study of Adsorbed Molecules on Metal Surfaces by Reflection Techniques. *The Journal of Chem. Phys.*, 44(1):310, Jan. 1966.
- [98] Y. Rotenberg, L. Boruvka, and A. W. Neumann. Determination of Surface Tension and Contact Angle from the Shapes of Axisymmetric Fluid Interfaces. *J. Colloid Interface Sci.*, 93(1):169, 1983.
- [99] P. Cheng, D. Li, L. Borukva, Y. Rotenberg, and A. W. Neumann. Automation of Axisymmetric Drop Shape Analysis for Measurement of Interfacial Tensions and Contact Angles. *Colloids and Surfaces*, 43:151, 1990.
- [100] D. Y. Kwok, D. Li, and A. W. Neumann. *Applied Surface Thermodynam-*

- ics*, volume 63 of *Surfactant science series*. Marcel Dekker, New York, 1996.
- [101] D. Y. Kwok, C. J. Budziak, and A. W. Neumann. Measurements of Static and Low Rate Dynamic Contact Angles by Means of an Automated Capillary Rise Technique. *J. Colloid Interface Sci.*, 173:143, 1995.
- [102] K. Isaacson, J. J. Blackstock, M.R. Freeman, and D. Y. Kwok. in preparation 2004.
- [103] R. Ragan, D. A. A. Ohlberg, R. S. Williams, J. J. Blackstock, and S. Kim. Atomic Surface Structure of UHV Prepared Template-Stripped Platinum and Single Crystal Platinum(111). *Journal of Physical Chemistry B*, submitted 2004.
- [104] D. J. Trevor, C. E. D. Chidsey, and D. N. Loiacono. *In-Situ* Scanning-Tunneling-Microscope Observation of Roughening, Annealing, and Dissolution of Gold (111) in and Electrochemical Cell. *Phys. Rev. Lett.*, 62(8):929, 1989.
- [105] W. Haiss, D. Lackey, J. K. Sass, and K. H. Besocke. Atomic resolution scanning tunneling images of Au(111) surfaces in air and polar organic solvents. *J. Chem. Phys.*, 95(3):2193, 1991.
- [106] R. Emch, J. Nogami, M. M. Dovek, C. A. Lang, and C. F. Quate. Characterization of gold surfaces for use as substrates in scanning tunneling microscopy studies. *J. Appl. Phys.*, 85(1):79, 1989.

- [107] D. Li and A. W. Neumann. Contact Angles on Hydrophobic Solid-surfaces and their Interpretation. *J. Colloid Interface Sci.*, 148:190, 1992.
- [108] H. W. Fox and W. A. Zisman. The Spreading of Liquids on Low-Energy Surfaces. 1. Polytetrafluoroethylene. *J. Colloid Sci.*, 5:514, 1950.
- [109] K. Grundke, S. Zschoche, K. Pöschel, T. Gietzelt, S. Michel, P. Friedel, D. Jehnichen, and A. W. Neumann. Wettability of Maleimide Copolymer Films: Effect of the Chain Length of *n*-Alkyl Side Groups on the Solid Surface Tension. *Macromolecules*, page 6768, 2001.
- [110] M. Kawasaki, T. Sato, T. Tanaka, and K. Takao. Rapid Self-Assembly of Alkanethiol Monolayers on Sputter-Grown Au(111). *Langmuir*, 16:1719, 2000.
- [111] D. Losic, J. G. Shapter, and J. J. Gooding. Influence of Surface Topography on Alkanethiol SAMs Assembled from Solution and by Microcontact Printing. *Langmuir*, 17:3307, 2001.
- [112] J. A. M. Sondag-Huethorst, C. Schönenberg, and L. G. J. Fokkink. Formation of Holes in Alkanethiol Monolayers on Gold. *J. Phys. Chem.*, 98:6826, 1994.
- [113] K. Kobayashi, T. Horiuchi, H. Yamada, and K. Matsushige. STM studies on nanoscopic structures and electric characteristics of alkanethiol and alkanedithiol self-assembled monolayers. *Thin Solid Films*, 331:210, 1998.
- [114] P. E. Laibinis, M. A. Fox, J. P. Folkers, and G. M. Whitesides. Comparisons of Self-Assembled Monolayers on Silver and Gold: Mixed Monolayers

Derived from $\text{HS}(\text{CH}_2)_{21}\text{X}$ and $\text{HS}(\text{CH}_2)_{10}\text{Y}$ ($\text{X}, \text{Y} = \text{CH}_3, \text{CH}_2\text{OH}$) Have Similar Properties. *Langmuir*, 7:3167, 1991.

- [115] C. D. Bain and G. M. Whitesides. Depth Sensitivity of Wetting: Monolayers of ω -Mercapto Ethers on Gold. *J. Am. Chem. Soc.*, 110:5897, 1988.
- [116] C. D. Bain and G. M. Whitesides. Molecular-Level Control over Surface Order in Self-Assembled Monolayer Films of Thiols on Gold. *Nature*, 240:62, 1988.
- [117] F. Frank. *Water: A Matrix of Life*. Royal Society of Chemistry, Cambridge, UK, 2 edition, 2000.
- [118] H. Tavana, C. N. C. Lam, K. Grundke, P. Friedel, D. Y. Kwok, M. L. Hair, and A. W. Neumann. Contact Angle Measurements With Liquids Consisting of Bulky Molecules. *J. Colloid Interface Sci.*, 279:493, 2004.